A comparative study of multi frequency kelvin probe force microscopy methods

by

Niklas Tausendpfund

Bachelorarbeit in Physik
vorgelegt dem Fachbereich Physik, Mathematik und Informatik (FB 08)
der Johannes Gutenberg-Universität Mainz
am 17. September 2016

1. Gutachter: Jun. Prof. Dr. Stefan Weber
2. Gutachter: Prof. Dr. Angelika Kuehnle

Ich versichere, dass ich die Arbeit selbstständig verfasst und keine anderen als die angegebenen Quellen und Hilfsmittel benutzt sowie Zitate kenntlich gemacht habe.

Mainz, den _____

Niklas Tausendpfund
Institut für Physik
Staudingerweg 7
Johannes Gutenberg-Universität D-55099 Mainz
ntausend@students.uni-mainz.de

Abstract

A lot of different Kelvin probe force microscopy methods were invented since the first method was presented by Nonnenmacher et al. in the early nineties. Since the nano scale distribution of surface potential becomes more and more interesting in terms of material science, e.g. for perovskite solar cells, the goal of this bachelor thesis was the implementation and comparison of four of these Kelvin probe force microscopy methods and test their reliability. The reproducibility of a applied voltage was tested with a reference sample consists of a gold electrode array. It was proved, that the closed loop methods were able to reproduce the excepted value within some percent, but the open loop methods showed a strong derivation from that value. During the further procedure some problems were identified with the aid of special analysis.
This work provides the beginning for a deeper understanding of modern methods to examine surface potentials, and therefore this work is interesting for further researches sector of modern solar cells, as the perovskite solar cells, and for doing measurements in fluids, since these techniques could be easy integrated in such a set-up.

Kurzzusammenfassung

Viele verschiede Formen der Kelvin Sonden Kraft Mikroskopie wurden entwickelt seid die erste Methode von Nonnenmacher et al. in den frühen Neunzigern vorgestellt wurde. Da die Oberflächenpotentialverteilung im nanometer Bereich immer mehr interessant wird für die Materialforschung, wie z.b. bei der Entwicklung von Perowskit Solar Zellen, war das Ziel der vorliegenden Bachelorarbeit vier verschiedene Formen der Kelvin Sonden Kraft Mikroskopie zu implementieren, diese miteinander zu vergleichen und auf ihre Zuverlässigkeit zu testen. Mit Hilfe einer Referenz Probe, einem Array aus Goldelektroden, wurde die Reproduzierbarkeit einer angelegten Spannung getestet. Es konnte gezeigt werden, dass die closed loop Methoden den erwarteten Wert gut reproduzieren, die open loop Methoden jedoch starke Abweichungen zeigten. Im weiteren Verlauf der Arbeit konnten einige der Probleme mit Hilfe spezieller Untersuchungen identifiziert werden.
Diese Arbeit liefert einen Anfang für ein zugrunde liegendes Verständnis moderner Methoden um Oberflächenpotentiale zu bestimmen und ist damit auch besonders interessant für weiterführende Arbeiten im Bereich der Analyse von modernen Solarzellen, wie Perowskit Solar Zellen, oder Stoffen in Flüssigkeiten, da diese Methoden leicht in ein solches Set-Up integriert werden können.

Der Kluge lernt aus allem und von jedem, der Normale aus seinen Erfahrungen und der Dumme weiß alles besser.

Sokrates

Table of Content

1. Introduction

The search for new strategies of producing renewable energies is one of the most important tasks in modern physic, since fossil fuels are restricted. One technique to produce clean energy is to use solar cells, which uses solar power to produce electrical energy. This process is called the photovoltaic effect and was first discovered by Alexandre Edmond Becquerel in 1839. After a lot of work was done in this sector, the first silicon p-n junction photocell was invented by D. M. Chapin et al. in 1954, [1]. Since the simple silicon p-n junction photocell is good understood, there are modern types of solar cells needed to be more examined. So one type of modern solar cells uses a perovskite material as the raw material, invented by Akihiro Kojima et al. in 2009, see [2], but this solar cell type shows some problems as a anomalous hysteresis in the measured current density against a applied bias voltage, see [3, 4]. To examine effects as this hysteresis a technique is required, which could measure the surface potential of a sample in the nano scale. That resolution is necessary, since perovsikte solar cells are not homogeneous and have a complex nano meter scale structure. So measuring the surface potential and analyse it in respect for significant fluctuation could lead to a hint of static charges trapped in defects, causing a high local electrical field.
The basic discovery used for the techniques used in this thesis was made by lord Kelvin, who found out, that there is a potential difference between two metals close to each over, called the contact potential difference, U_{CPD}. This contact potential difference only depends on the energy, that is needed to remove a electron from the highest electrical state into the vacuum state, called the working function. Lord Kelvin also invented a technique to measure this contact potential difference, the Kelvin probe microscope, see [5]. However, this technique do not provide the necessary spatial resolution. The solution is to combine lord Kelvins method with the atomic force microscope, invented in 1986 [6], in a dynamical mode. This was first presented in 1991 by Nonnenmacher et al., see [7], called the **Kelvin probe force microscope**. Up to now there are a lot of different ways invented to perform a KPFM measurement, as methods with feedback loops, e.g. the heterodyne method, [8] or open loop methods, [9, 10]. The advantage of these open loop methods are, that they could be applied to a measurement in fluid, since the high damping factor of the fluid causes a reduction of the oscillation, so that the amount of cross talking subsystems should be reduced, to provide a stable signal. Therefore the open loop methods can be used to measure changes in the surface potential e.g. caused by chemical reactions or to get electrical properties of polymer solutions etc.
So to get qualitative information out of a system a accurate understanding of the used measurement method is required, so this thesis had the aim to implement different types of Kelvin probe force microscopy, compare them in respect to the reliability and to identify possible problems and limits.

2. Theory

The atomic force microscope (**AFM**) is used to measure the force between a nano scale tip and a surface, like the van-der-Waals or electric static forces. In this chapter there is a short introduction to the theory of the atomic force microscope and the Kelvin probe force microscope (**KPFM**), which is used to measure the contact potential difference U_{CPD}.

2.1. Atomic Force Microscopy

To detect the forces, which acts near a surface on a tip, a micrometer sized cantilever structure is used with a tip of the order of a few nano meters on its free end (see figure B.8, on page 42).
This cantilever can be seen in the first approximation like a hooke's spring (for deeper analysis the Euler Bernoulli beam theory is required, [11]):

$$F = k \cdot s \tag{2.1}$$

In which k stands for the spring constant and s for the deflection out of the equilibrium state. That means, that the force acting on the tip, can be simply measured by detecting the deflection, e.g. align a laser beam on the tip and measure the reflected light by a photodiode (see picture 2.1).
In this work a dynamic mode of atomic force microscope was used. That means, the cantilever was mechanically excited with a piezo element on the frequency ω_m. The following equation of motion can be found for a free damped oscillation:

$$\frac{1}{\omega_0^2}\ddot{s}(t) + \frac{1}{Q\omega_0}\dot{s}(t) + s(t) = F_{drive,\omega_m}(t) \tag{2.2}$$

With ω_0: Resonance frequency of the undamped oscillation, Q: quality factor of the oscillation, describing the amount of energy, which is lost during one oscillation, $F_{drive,\omega_m}(t)$ is the driving force acting on the frequency ω_m, which is most of the times of the form $A_0 \cdot \cos(\omega_m t + \phi_m)$. After a Fourier transform the following equation can be derived:

$$(-\frac{\omega_m^2}{\omega_0^2} + \frac{i\omega_m}{Q\omega_0} + 1)^{-1}\hat{s}(\omega_m) = \hat{F}_{drive}(\omega_m) \tag{2.3}$$

The function

$$\chi(\omega) = (-\frac{\omega_m^2}{\omega_0^2} + \frac{i\omega_m}{Q\omega_0} + 1)^{-1} \tag{2.4}$$

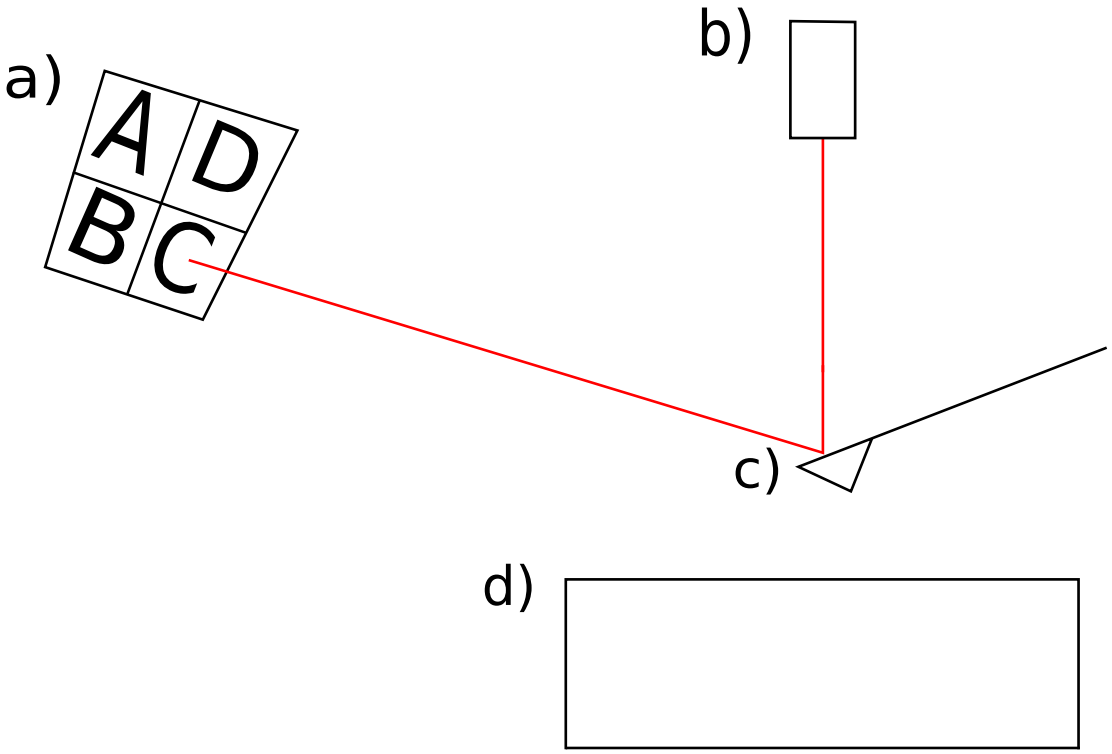

Fig. 2.1.: Scheme of a atomic force microscope. **a)** A four field photo diode to detect the deflection of the laser beam. To get the lateral deflection: $(I_A+I_B)-(I_D+I_C)$, vertical deflection: $(I_A + I_D) - (I_B + I_C)$, with I_n: photo current of the nth photo diode field. **b)** Laser beam source, focused on the top of the cantilever. **c)** Cantilever, driven by a piezo for a mechanical excitation. **d)** Sample

is called the transfer function of the system, and determines, how a the cantilever reacts, if a force acts on the frequency ω.
Now an additional weak force field is acting on the cantilever. That means, $F_{ext}(s = 0) = 0$, since in the equilibrium state $s = 0$ there should be no force acting on the cantilever, and $\frac{\partial F_{ext}}{\partial z}(s = 0) \ll 1$. This force field could be for an example a Lennard Jones potential. This leads to an additional force term in equation 2.1:

$$\begin{aligned} F &= k \cdot s - F_{ext}(z) && (2.5)\\ &= k \cdot s - \frac{\partial F_{ext}}{\partial z}(s = 0) \cdot s && (2.6)\\ &= k_{eff} \cdot s && (2.7) \end{aligned}$$

So in our equations of motions we need to substitute $\omega_0 \rightarrow \omega_{0,eff}$. To measure the topography of the sample, a feedback is applied, which controlled the tip sample distance, so the tip felt the same force all the time. This could be done by holding the amplitude on a constant value, since force and amplitude are connected through the equation 2.3.

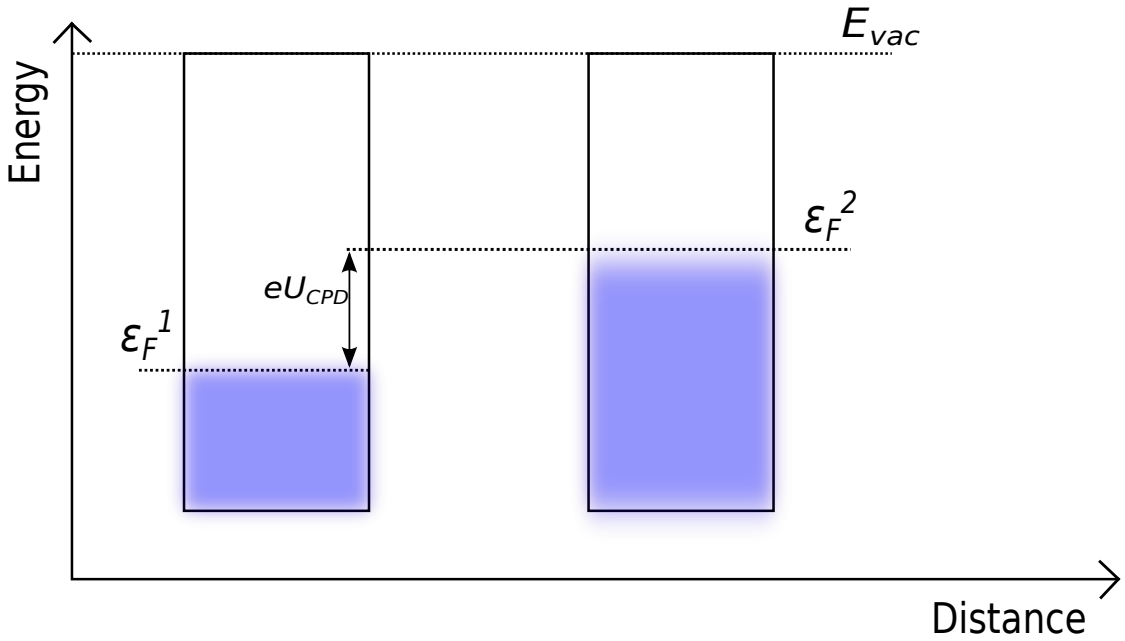

Fig. 2.2.: The contact potential difference of two metals is defined through the difference of the Fermi levels of the two metals, ϵ_F^1 and ϵ_F^2. The Fermi level of a metal is the energy of the highest occupied quantum mechanical state, [12, 13], [14, pp. 19-20].

2.2. Kelvin Probe Force Microscopy

The aim of this thesis is to implement and compare different types of measuring the contact potential difference (U_{CPD}) of a surface with an **AFM** set-up. This is called the **Kelvin probe force microscope** (**KPFM**).
The U_{CPD} is defined as the difference of the work function of two materials. In the simple cases for two metals this is described by the difference of the Fermi levels, see picture 2.2:

$$e \cdot U_{CDP} = \epsilon_2 - \epsilon_1 \tag{2.8}$$

A simple method to measure the U_{CPD} is the Kelvin probe, developed by Lord Kelvin in 1898, [5]. In this method a probe with a given work function is used. This probe then vibrates near to the sample, leading to a electric current flowing to the probe, since the probe sample can be descried by a capacitor. This current can then be nullified by a constant U_{bias}, which is then equal to the U_{CPD}. But this technique suffers from a bad spatial resolution, since you need a probe with a big capacity, and therefore a big area, which leads to an average of the U_{CPD} over a big area, to get measurable electric currents. To get a high spatial resolution, the tip of an **AFM** can be used, but a different method is required, since the electric current is too low to be measurable. The

tip-sample system can still be described by a capacitor:

$$F = \frac{1}{2} \cdot \frac{\partial C}{\partial z} \cdot (\Delta U)^2 \tag{2.9}$$

Where C is the capacity of the tip-sample system as a function of the distance z and ΔU is the potential difference between the tip and the sample. If we consider the tip-sample system as a capacitive system, and apply an additional potential on the tip, the total potential difference is given by:

$$\Delta U = U_{CDP} - U_{ext} \tag{2.10}$$

where U_{ext} has the following form:

$$U_{ext} = U_{AC} \cdot \cos(\omega_E t + \phi_E) - U_{bias} \tag{2.11}$$

With the amplitude U_{AC} of the excitation at the frequency ω_E, ϕ_E the phase between the electrical excitation and the reference signal of the lock-in amplifier and U_{bias} a constant offset.
Putting 2.10 in the expression for the force 2.9 leads to the following (w.l.o.g. $\phi_E = 0$):

$$F = \frac{1}{2} \cdot \frac{\partial C}{\partial z} \cdot (U_{CPD} - U_{bias} + U_{AC} \cdot \cos(\omega_e))^2$$

This leads to, by expanding and reordering:

$$F_{stat} = \frac{1}{2}\frac{\partial C}{\partial z}\left((U_{CPD} - U_{bias})^2 + \frac{U_{AC}^2}{2}\right) \tag{2.12}$$

$$F_{\omega_E} = \frac{\partial C}{\partial z}(U_{CPD} - U_{bias})U_{AC}\sin(\omega_E t) \tag{2.13}$$

$$F_{2\omega_E} = \frac{1}{4}\frac{\partial C}{\partial z}U_{AC}^2\cos(2\omega_E t) \tag{2.14}$$

2.2.1. Closed Loop Amplitude Modulation

The first method for measuring the U_{CPD} was the Amplitude Modulation, presented by Nonnenmacher et al. 1991 [7]. This technique uses the fact, that the response of the cantilever on the frequency ω_E is proportional to the difference between U_{CPD} and U_{bias}. This can be easily seen by using F_{ω_E} from equation 2.13 as an additional force acting on the cantilever. Since this force is proportional to a sinusoidal function, the cantilever begins to oscillate with the same frequency. By minimizing the amplitude of the ω_E signal the following equation holds:

$$U_{bias} = U_{CPD} \tag{2.15}$$

That means, by tracking the bias voltage which is needed to nullify the amplitude with a feedback the contact potential difference between the surface and the tip is measured.

2.2.2. FM/Heterodyne

As discussed in the section 2.1 a weak force field causes a shift of the spring constant of the cantilever, equation 2.7, and therefore changes the first resonance frequency of the cantilever as follows:

$$\tilde{\omega}_0 = \sqrt{\frac{k - \partial F/\partial z}{m_{eff}}} \approx \omega_0 (1 - \frac{1}{2k}\frac{\partial F}{\partial z}) \tag{2.16}$$

with $\omega_0 = \sqrt{\frac{k}{m_{eff}}}$ being the resonance frequency of the undisturbed cantilever.
Using the derivation of the force 2.13 as the force gradient in 2.16 the following equation for the frequency shift occurs:

$$\tilde{\omega}_0(t) \approx \omega_0 (1 - \frac{1}{2 \cdot k}\frac{\partial^2 C}{\partial z^2}(U_{CPD} - U_{bias})U_{AC}\sin(\omega_E t)) \tag{2.17}$$

Since $s(t) = A_0 \cdot \cos(\int_{t_0}^{t} \tilde{\omega}_0(t')\,dt')$ is a solution for the differential equation, which describes the deflection of the cantilever:

$$\ddot{s}(t) = (\tilde{\omega}_0(t))^2 \cdot s(t)$$

We can find, with $\tilde{\omega}_0(t)$ as defined in 2.17:

$$\begin{aligned} s(t) &= A_0 \cdot \cos(\int_{t_0}^{t} \tilde{\omega}_0(t')\,dt') \\ &= A_0 \cdot \cos(\omega_0 t + \frac{\delta\omega}{\omega_E} \cdot \sin(\omega_E t) + \phi_0) \end{aligned} \tag{2.18}$$

In wich

$$\delta\omega = \frac{\omega_0}{2 \cdot k}\frac{\partial^2 C}{\partial z^2}(U_{CPD} - U_{bias})U_{AC} \tag{2.19}$$

After expanding this into a Fourier-sum, assuming that $\frac{\delta\omega}{\omega_E} \ll 1$, only take the first two terms of the sum into account, and setting w.l.o.g. $\phi_0 = 0$, the deflection can be written as:

$$\frac{s}{A_0} \approx \cos(\omega_0 t) + \frac{\delta\omega}{\omega_E} \cdot (\cos((\omega_0 + \omega_E)t) - \cos((\omega_0 - \omega_E)t)) \tag{2.20}$$

The derivation of this equation is done in the appendix A. Taking into account, that $\delta\omega$ is proportional to $U_{CPD} - U_{bias}$, it is possible to apply a feedback, that nullifies one of the Amplitudes at $\omega_0 \pm \omega_E$, leading to $U_{CPD} = U_{bias}$. This method is called frequency modulation (FM) (Zerweck et al. [15]) or heterodyne KPFM (Joseph et al. [8]). It was shown that the spatial resolution of methods using the frequency shift is better than the resolution with the AM technique, [15]. Also the weight function for charges sitting on the surface is different for the both techniques, as calculated in [16], which comes from the fact, that the AM KPFM is sensitive for the capacitive gradient, and the heterodyne KPFM is sensitive for the second derivative of the capacity. Since only the force acting on the frequency ω_E was taken into account, there is a big approximation neglecting the static force and the $2\omega_E$ force.

2.3. Open Loop Methods

Due to the high damping factor of water, causes a quality factor decreasing by 2 orders of magnitude, measurements of the surface potential of samples in water with a KPFM requires a special technique. Since the amplitude of the oscillation of the cantilever is quite small, this technique should perform without an additional feedback, so that the amount of interfering feedback loops is reduced to the distance feedback. Turing off the feedback is mathematically equivalent to set the constant bias voltage U_{bias} in equation 2.11 to zero. Driving a cantilever near to his resonance frequency, $\omega_m \approx \omega_0$, the position of the cantilever can be described approximately with:

$$z(t) = h + A_D \cos(\omega_m t + \phi_m)$$

with h being the equilibrium position and A_D the amplitude of the deflection. This approximation only holds if the cantilever does not jump into contact with the surface. To get further a slow electrical excitation is required, [9].
Since the capacity is a function of the tip-sample-distance, which is a periodic function in time, we can also assume, that the capacity itself is a periodic function in time with the same frequency:

$$\frac{\partial C}{\partial z}(t + \frac{2\pi}{\omega_m}) = \frac{\partial C}{\partial z}(t)$$

Using this identity there is a easy way to derive the equations for the open loop methods, which is an alternative derivation as the one presented by Borgani et al. [9]. Because the capacity is periodic in time with the frequency ω_m it can be expanded into the following Fourier sum, w.l.o.g. $\phi_m = 0$:

$$\frac{\partial C}{\partial z}(t) = \sum_{n=-\infty}^{\infty} c_n e^{in\omega_m t}$$

Since the gradient of C is a real and symmetric function, because $z(t)$ is a symmetric function, the equation can be written as:

$$\frac{\partial C}{\partial z}(t) = \sum_{n=0}^{\infty} a_n \cos(n\omega_m t) \tag{2.21}$$

with the real Fourier-coefficients a_n. Now putting equation 2.21 in equation 2.9 the following forces can be found, neglecting the constant terms and the terms with $n > 1$:

$$F_{\omega_E} = a_0 U_{CPD} U_{AC} e^{i\phi_E} \tag{2.22}$$
$$F_{2\omega_E} = \tfrac{1}{4} a_0 U_{AC}^2 e^{2i\phi_E} \tag{2.23}$$
$$F_{\omega_m \pm \omega_E} = \tfrac{1}{2} a_1 U_{CPD} U_{AC} e^{\pm i\phi_E} \tag{2.24}$$
$$F_{\omega_m \pm 2\omega_E} = \tfrac{1}{8} a_1 U_{AC}^2 e^{\pm 2i\phi_E} \tag{2.25}$$

Starting from this equations, two independent equations for U_{CPD} can be derived:

$$U_{CPD} = \frac{U_{AC}}{4} \frac{F_{\omega_E}}{F_{2\omega_E}} e^{i\phi_E} \tag{2.26}$$

$$U_{CPD} = \frac{U_{AC}}{4} \frac{F_{\omega_m \pm \omega_E}}{F_{\omega_m \pm 2\omega_E}} e^{\pm i\phi_E} \tag{2.27}$$

Equation 2.26 describes the AM open loop method and equation 2.27 the FM open loop method. It is also possible to derive the capacity gradient and the second derivation of the capacity, since the Fourier coefficient a_0 and a_1 are proportional to the first and second derivative of the capacity respectively. This also means, that the ω_E and $2\omega_E$ force are proportional to the first derivation of the capacity, as the force in the closed loop AM, and the $\omega_m + \omega_E$ and $\omega_m + 2\omega_E$ forces are proportional to the second derivative of the capacity as the force of the heterodyne method.
Since the lock-in amplifier only measures amplitudes and not forces as it is required for 2.26 and 2.27, the amplitude needs to be corrected by the ratio of the transfer function, because the forces and amplitudes are linked through the transfer function, see equation 2.4. The equations changes then to:

$$U_{CPD} = \frac{U_{AC}}{4} \frac{g(2\omega_E)}{g(\omega_E)} \frac{A_{\omega_E}}{A_{2\omega_E}} e^{i\phi_E} \,. \tag{2.28}$$

$$U_{CPD} = \frac{U_{AC}}{4} \frac{g(\omega_m \pm 2\omega_E)}{g(\omega_m \pm \omega_E)} \frac{A_{\omega_m \pm \omega_E}}{A_{\omega_m \pm 2\omega_E}} e^{\pm i\phi_E} \tag{2.29}$$

where $g(\omega)$ is the real amplitude of the complex transfer function $\chi(\omega)$. For the driven damped harmonic oscillator it hast the following form:

$$g(\omega) = \frac{A}{\sqrt{(\omega_0^2 - \omega^2)^2 + (\frac{\omega_0 \cdot \omega}{Q})^2}} \tag{2.30}$$

with the quality factor Q and a general amplitude A, which depends on the spring constant of the cantilever and the sensitivity of the system.

2.4. Lock-In-Amplifier

In this section will be a short introduction to the basics of a lock-in amplifier. This device provides the possibility to measure small amplitudes compared to the noise level. The amplifier first multiplies the incoming measurement signal with a sinusoidal reference function with frequency ω_{ref}, which is phase shifted by $\Delta\phi$, and then multiplies this product over a certain time τ, the time constant:

$$U_{out}(t) = \frac{1}{\tau} \int_{t-\tau}^{t} \sin(\omega_{ref} \cdot \tau + \Delta\phi) U_{in} \, d\tau$$

Increasing the time constant would lead in lesser noise, but also in lesser accuracy. A scheme of a lock-in-amplifier is showed in 2.3. By a good choice of the integration time this technique filters frequency bands out of a noise signal, allowing to perform KPFM, since the signals on a certain frequencies are rather small.

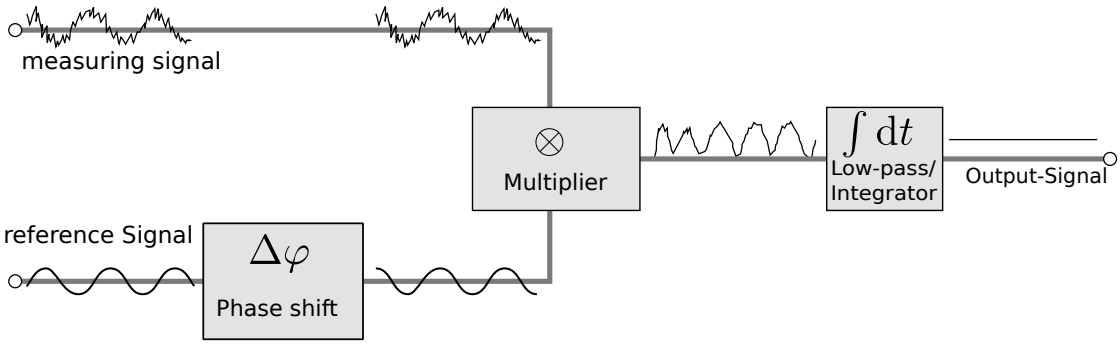

Fig. 2.3.: Scheme of the working principle of a lock-in amplifier, downloaded from wikipedia.de on the 15.11.2016, description changed to English afterwards.

3. Set Up

3.1. System

The measurements were performed on a JPK nanowizard III set-up combined with a Zurich Instruments lock-in amplifier of the type HF2LI. The distance feed-back was performed by the JPK controller, the kelvin probe measurements by the lock-in amplifier, controlled by the software allocated by Zurich Instruments. The analysis was done with Gwyddion (www.gwyddion.net) and Python. The measurements were performed with platinum-iridium coated cantilever. The properties can be seen in table 3.1, a picture of the cantilever can be seen in the appendix B.8. The model number of them is SCM-PITW.

3.2. Sample

The sample was a electrode array structure made by ALS, Japan. Only the two working electrodes were used, with one of them set to ground potential, the other one to a higher potential.

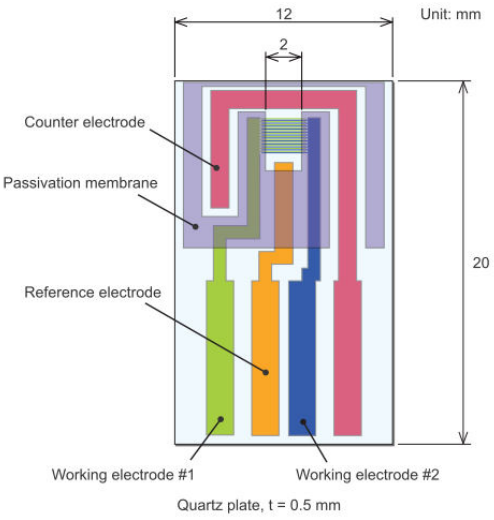

Fig. 3.1.: Scheme of the electrode structure (downloaded from www.als-japan.com/ on the 11.10.16.)

The sample was a electrode array structure made by ALS, Japan. Only the two working electrodes were used, with one of them set to ground potential, the other one to a higher potential. The electrodes was made of gold, the surrounding material was glass. This sample was chosen, because of the possibility to have a clearly defined potential distribution on a small range, which could be controlled during the measurements with an external instrument. It also has a nearly flat topography on the glass as it can be seen in fig. 3.2, but the height falls rapidly on the edge to an electrode. Also the measured U_{CPD} used to overshoot on the edge to an electrode with a high potential, as it can be seen in fig. 3.3(d). This effect was observed by all methods, but since the focus of this work was on the implementation and comparing of the different methods, there was

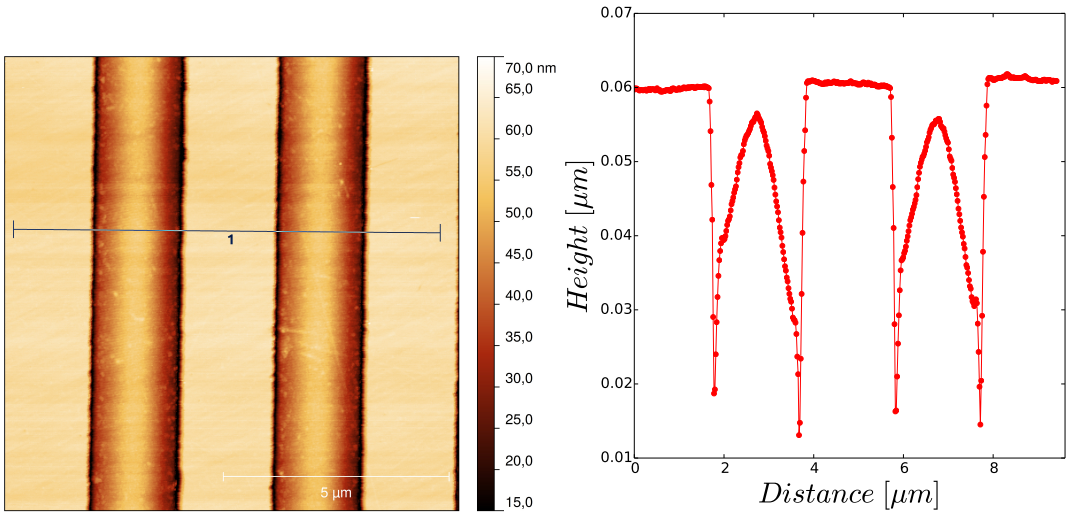

(a) 2D scan (b) Cross-section

Fig. 3.2.: A AFM scan of the surface. The conic parts in the cross-section are the electrodes, the flat parts the glass.

not a closer look taken on this phenomena.
The electrodes were separated by $2\,\mu m$ and their width amounted $2\,\mu m$. The potential differences was provided by the lock-in amplifier through two clamps, which were in contact with the two electrode respectively.
If a U_{CPD} distribution was measured over a area containing more then 3 electrodes, the applied voltage can be calculated by averaging the U_{CPD} over the electrodes with high potential and subtracting the averaged U_{CPD} from the electrodes with the low potential, because of:

$$\begin{aligned} \Delta\overline{U}_{CPD} &= \overline{U}_{CPD,high} - \overline{U}_{CPD,low} \\ &= \overline{U}_{CPD,gold} - \overline{U}_{CPD,gold} + \Delta\overline{U}_{ext} \\ &\approx \Delta\overline{U}_{ext} \end{aligned}$$

For some measurements in section 4.2 a graphite sample was used, because of a almost homogeneous surface, providing homogeneous conditions on a large area.

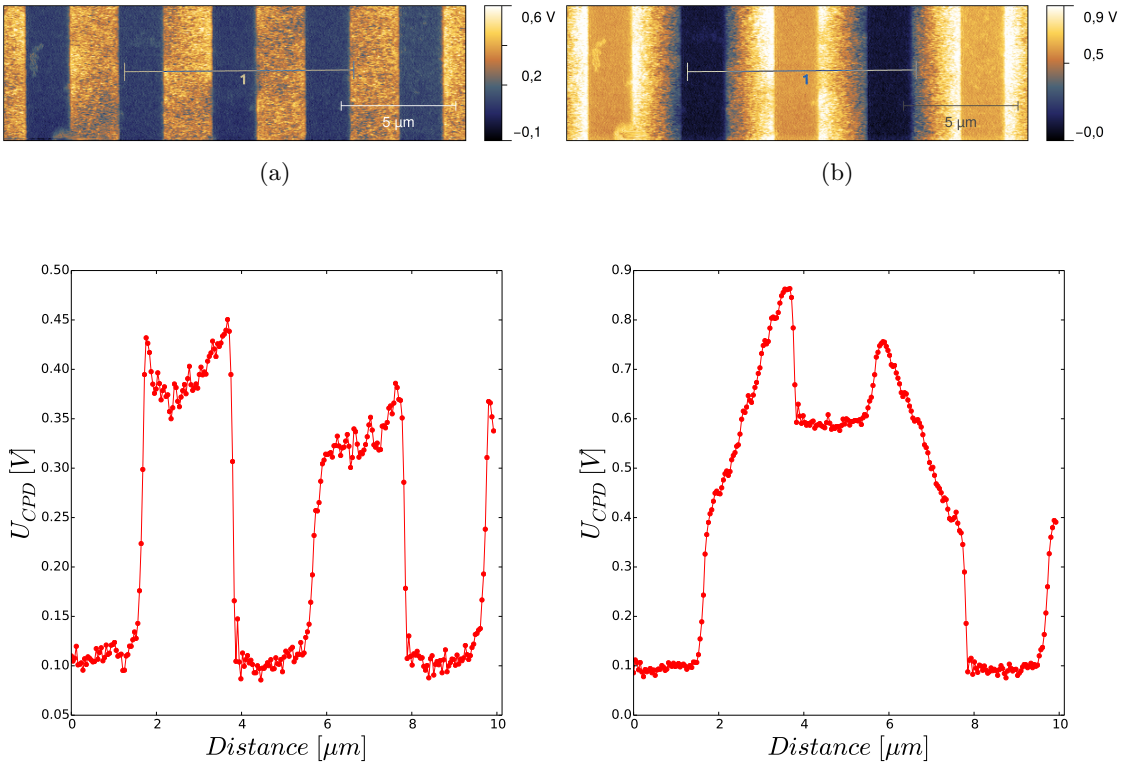

(a) (b)

(c) (d)

Fig. 3.3.: In (a) the U_{CPD} was measured without an additional voltage on the electrodes, in (c) the cross section is plotted. In (b) a potential difference of $500mV$ was applied, in (d) the corresponding cross section. The overshoot on the edges of the electrode with the high potential can be clearly seen in (d).

properties	value
width	23–33 μm
length	200–250 μm
thickness	2.5–3. μm
resonance frequency	60–100 kHz
spring constant	1–5 $\frac{N}{m}$

Table 3.1.: The properties of the used cantilever

3.3. Implementation of the Methods

For the implementation of the methods one basic set-up can be used, shown in fig. 3.4. So for a better overview all of the methods are listed in the table 3.2, with the excitation and detection frequencies. ω_1 stands for the second eigenmode of the cantilever, which is used to record the closed loop methods, since the response off the system should be higher. Since the electrical feedback could be controlled with the software provided by Zurich Instruments, the needed U_{bias} could be streamed via the auxiliary output of the lock-in amplifier. In table 3.3 the relevant configurations of the lock-in amplifier are listed.

method	electrical excitation	detection frequency	feedback
AM, closed loop	$\omega_E = \omega_1$	ω_1	on
Heterodyne	$\omega_E = \omega_1 - \omega_0$	ω_1	on
AM, open loop	$\omega_E \ll \omega_0$	ω_E and $2\omega_E$	off
FM, open loop	$\omega_E \ll \omega_0$	$\omega_0 \pm \omega_E$ and $\omega_0 \pm 2\omega_E$	off

Table 3.2.: The most important information for the different methods. ω_1 stands for the second eigenmode of the cantilever.

method	output 1	output 2	adder
AM, closed loop	U_{bias}	residual amplitude on ω_E	on
Heterodyne	U_{bias}	residual amplitude on ω_1	on
AM, open loop	ω_E	$2\omega_E$	off
FM, open loop	$\omega_0 \pm \omega_E$	$\omega_0 \pm 2\omega_E$	off

Table 3.3.: Configuration of the lock-in amplifier for the different methods

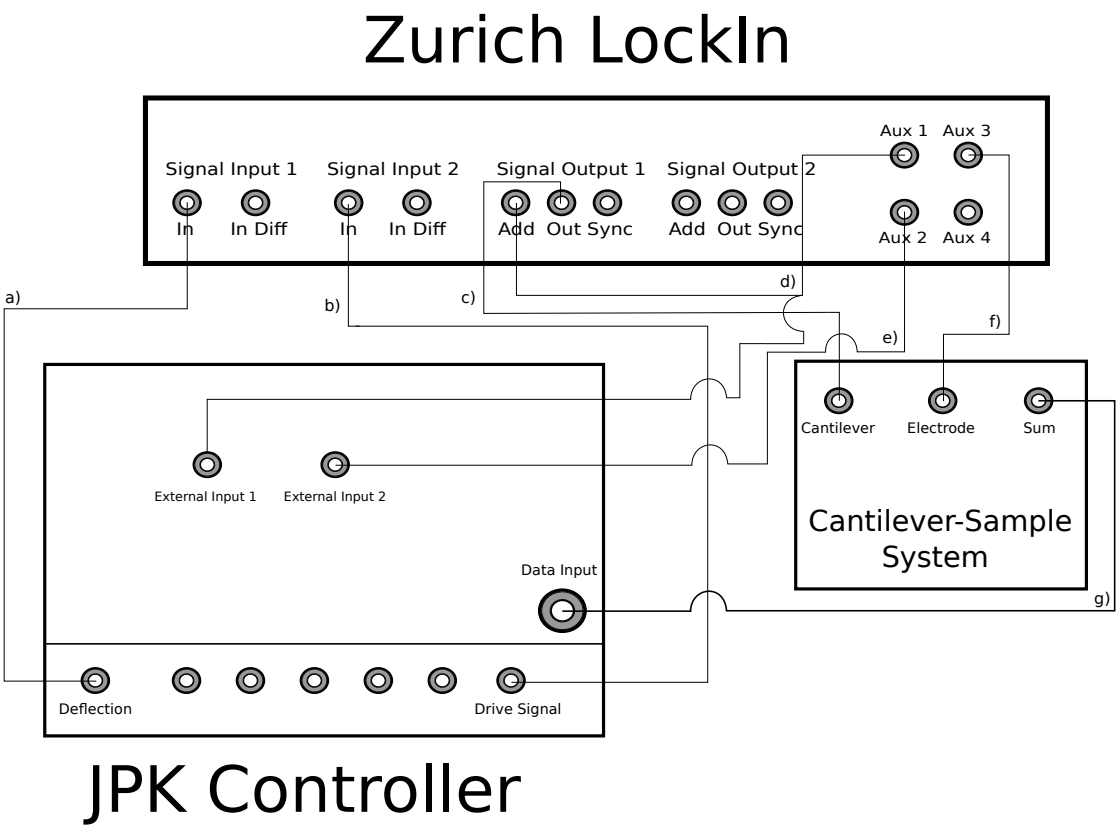

Fig. 3.4.: A scheme of the general set-up. a) Cable providing the deflection information measured by the JPK controller to the lock-in amplifier. b) Cable providing the drive signal information applied on the cantilever to the lock-in amplifier. c) Connection to the cantilever, for applying the external voltage $U_{ext}(t)$. d) This cable has two tasks, first it connects the lock-in amplifier output to a input of the JKP controller, used to display measured values. Secondly it also connects to the adder of the signal output 1, this connection is used for the feedback of the closed loop methods. For the open loop methods the adder should be disabled. e) Connection of the second out put of the lock-in amplifier to a input of the JPK controller. For the closed loop methods used for recording a error signal, for the open loop methods used for recording the amplitude on the second needed signal. f) This connection is used to apply the potential difference on the electrodes. See 3.5 for a deeper description of the cantilever-sample system. g) Cable providing the detected sum signal of the four field diode to the JPK controller.

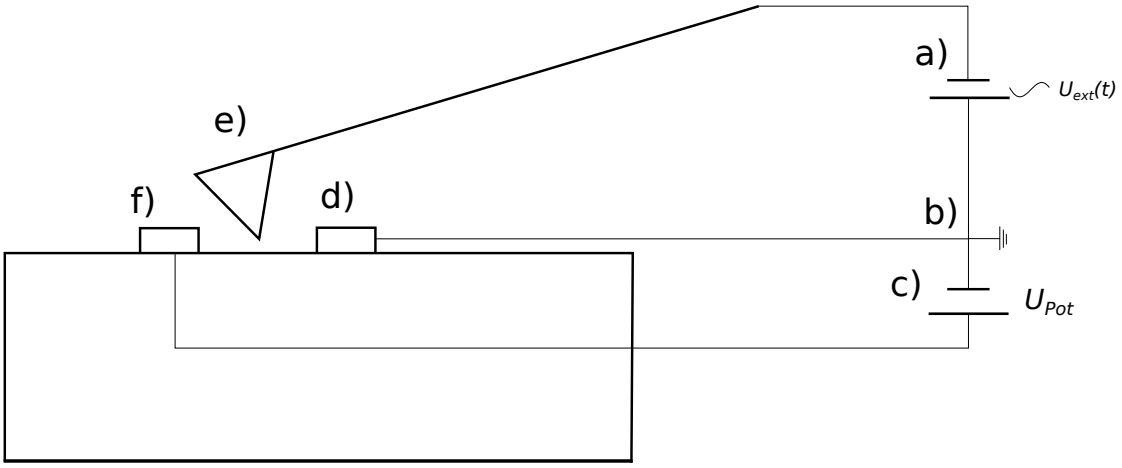

Fig. 3.5.: Scheme of the cantilever-sample system in KPFM a) The external voltage applied between the tip and the sample caused by the lock-in amplifier. b) shared ground of the tip and the sample. c) Source for the potential between the different electrodes, caused by the lock-in amplifier. d) Electrode on the ground potential. e) Cantilever, perpendicular aligned to the electrode beam. f) Electrode on the high potential.

4. Results and Discussion

4.1. Linearity

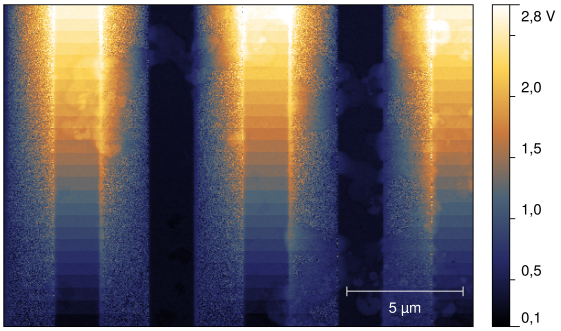

Fig. 4.1.: Increasing voltage on one electrode, measured with the heterodyne method

In order to test the reliability of the different methods, increasing voltages were applied to the electrodes of the sample measured by the different ways. The optimal performance for the measured voltage plotted against the applied voltage would be a straight line with the slope of one. The voltage was varied from $0\,V$ to $3.8\,V$ in steps of $100\,mV$ ever 25 scan lines, an example of a measurement preformed in this way is shown in 4.1, the other measurements are listed in B.1. The configuration for the single measurements are listed in the table 4.1. To get the average for the contact potential difference, cross sections perpendicular to the electrodes were taken for every voltage step, with an parallel averaging of 15 points. Then the high and low potential of every cross section was averaged over the associated electrodes. The resulting potential difference was then plotted against the applied voltage in the fig. 4.2 for every method, also the line for a perfect measurement was plotted (blue line). This plot shows a linear relationship for all methods over the whole range of $3.8\,V$, and therefore a linear fit could be performed to get the slopes, which are listed in the table 4.2. The best result with a slope of 0.929 was obtained for the heterodyne method, followed by the closed loop AM method with 0.812. The largest deviation was observed for the open loop AM method with 0.464 and the slope of the open loop FM method was 20% to high.

method	ω_m $[kHz]$	ω_E $[kHz]$	U_{AC} $[V]$
AM, closed loop	66.35	414.47	4
Heterodyne	72.9	386.37	4
AM, open loop	66.35	5	4
FM, open loop	72.9	3	4

Table 4.1.: Configuration for the voltage sweep measurements, ω_m, ω_E: mechanical and electrical excitation frequency, U_{AC}: AC excitation amplitude

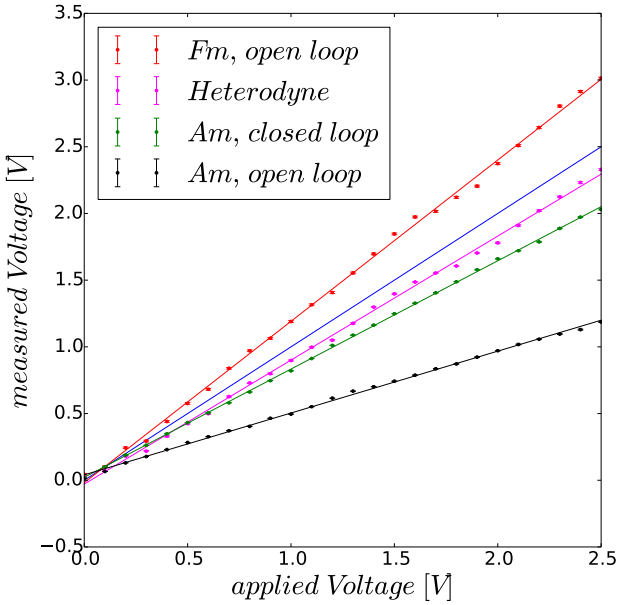

Fig. 4.2.: measured voltage from the different methods by applying increasing Ac voltages.

Method	Slope	r^2
Am closed loop	0.812 ± 0.003	0.9998
Heterodyne	0.929 ± 0.007	0.9987
Am open loop	0.464 ± 0.003	0.9988
Fm open loop	1.209 ± 0.009	0.9987

Table 4.2.: Slopes of the fits in the potential sweep from figure 4.2

The strong variance of slopes of the open loop methods from the close loop methods, and explicitly from the perfect slope of one, could have multiple origins. For example, the ratio of the transfer function could be more complex as assumed with the transfer function of a driven damped harmonic oscillator, equation 2.30. There could be another frequency dependent function $d(\omega)$ modulating the old transfer function $g(\omega)$ in the following way:

$$g(\omega) \rightarrow \tilde{g}(\omega) = g(\omega) \cdot d(\omega) \tag{4.1}$$

This modulation would lead to different weighting of the forces as they there treated in the calculations above. Another possibility could be cross talk between the the different subsystems, since the mixing products $\omega_m + \omega_E$ and $\omega_m + 2\omega_E$ were close to the first resonance peak, where the distance feedback was performing, and the bandwidth of this feedback loop could not be controlled. A third error could occur though the missing electric phase information. The phase of the electrical signal was set to zero at the beginning, but for a not scanning situation with high AC voltages. So during the measurement this phase could varied strong from zero, which would lead to an additional phase factor of $\cos(\phi_E)$.

4.2. Testing the Theory of Open Loop FM

To identify the problems with the problems for the open loop FM method, the dependency of the two side bands, $\omega_m + \omega_E$ and $\omega_m + 2\omega_E$, was analysed respectively to the applied AC voltage. The two equations, 2.24 and 2.25, predict a linear behaviour for the amplitude of the first side band in terms of increasing AC voltage, and a quadratic behaviour for the amplitude of the second side band. So a measurement was designed, where the tip was positioned over the electrode with the high potential, while $500\,mV$ potential difference was applied to the electrode array. While the cantilever was fixed on this position, it was excited mechanically with $64.7kHz$ and electrically at different frequencies and with various AC excitation amplitudes. This was controlled by a script, C.1, using the Zurich Instruments lock-in amplifier. This script collected the information of the amplitudes over five seconds at a certain AC excitation amplitude and electrical frequency, then the script switched the AC excitation amplitude one step higher, starting from $0\,V$ to $4.9\,V$ in $100\,mV$ steps, until the boundary AC excitation amplitude was reached. In the plot 4.3 the amplitude data collected in this way are plotted for an electrical excitation frequency of $4\,kHz$ and $5\,kHz$.

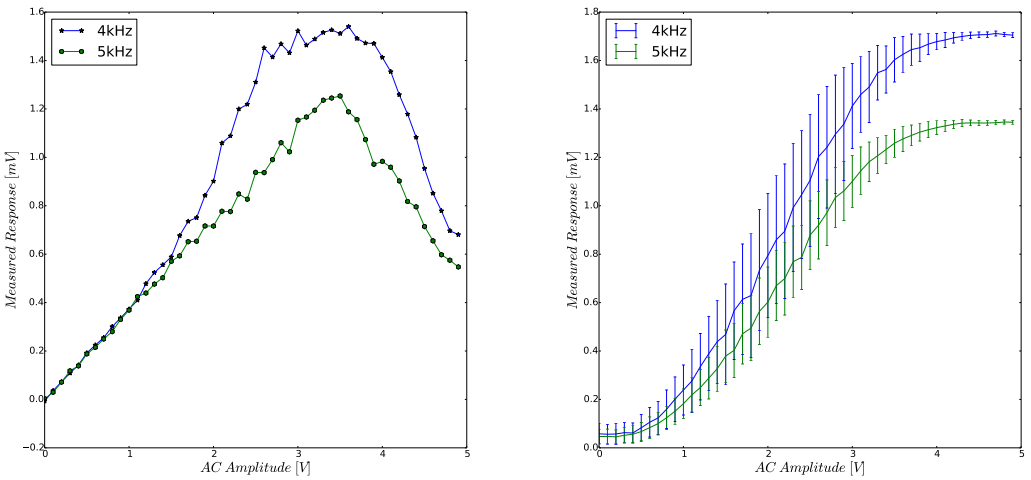

(a) (b)

Fig. 4.3.: The measured Response on the first and second side band vs different applied AC excitation amplitudes: (a) signal on $\omega_m + \omega_E$ and (b) signal on $\omega_m + 2\omega_E$. Measured while the tip was positioned over the electrode with the high potential.

The expected behaviour could only be seen up to a critical Ac voltage around $3.5\,V$. The amplitude of the $\omega_m + \omega_E$ signal reached a maximum and then decreased. The amplitude of the $\omega_m + 2\omega_E$ signal began to saturate to a maximum value of $1.34\,V$, by an excitation frequency of $5\,kHz$ and $1.7\,V$ at $4\,kHz$. Since the critical AC excitation amplitude was for both frequencies around the same value, the saturation seems not to be strongly dependent of the frequency.
Because of the small distance of the signal amplitude, $\omega_m + \omega_E$, to the mechanical excitation frequency, on which the distance feedback performed, crosstalk between the distance feedback and the side band detection could occur. That means, that the distance feedback detected the amplitude of the $\omega_m + \omega_E$ signal, summed this amplitude to the amplitude of the cantilever caused through the mechanical excitation. The feedback would tries to compensate this additional side band signal. This effect is expected to be higher for increasing AC voltages, since the amplitude increases with increasing AC voltages.
To test this hypothesis a different set up was used, the low noise set up. The low noise atomic force microscope is a home-build atomic force microscope, with a high signal to noise ratio, due to special designed electrical components. The advantage of this set up was the possibility to have a better control over the distance feedback during the measurements. To get comparative results a graphite sample was measured in the same way as the gold sample described above on both set ups. During the measurements on the low noise AFM, the feedback gains were set to the zero, ont the JPK set up that was not possible. In the fig. 4.4(a) and 4.4(b) the result for the measurement on the JPK set up were plotted. The behaviour of the two side bands at different AC voltages on the graphite sample looks similar to the behaviour on the gold sample, with the difference of the sign of the slope, for the graphite sample its negative. Also the critical AC voltage is different from the one measured on the gold sample.
Another behaviour can be seen in fig. 4.4(c) and 4.4(d), where the results of the measurement on the low noise set up were plotted. For the first side band, a linear relationship between the first side band and the AC voltage could be observed over the whole range of $5\,V$ for all the different electrical excitation frequency. The same holds for the second side band with a quadratic relationship. Based on this result the expectation of a feedback problem in the JPK set up seems to be reasonable. Since this effect would only change the total resulting value of a measured U_{CPD} this have not to be taken into account for pictures, in which the absolute value of the U_{CPD} is a matter.

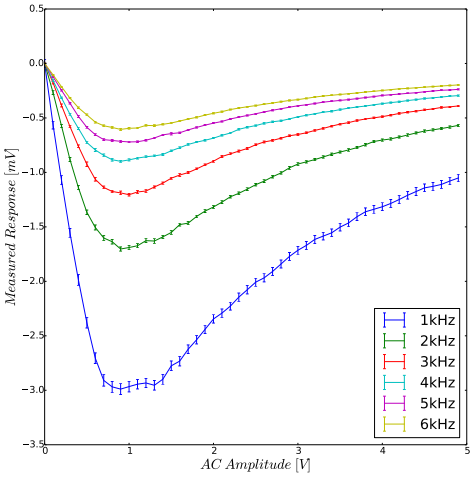

(a) $\omega_m + \omega_E$, JPK nano wizard III

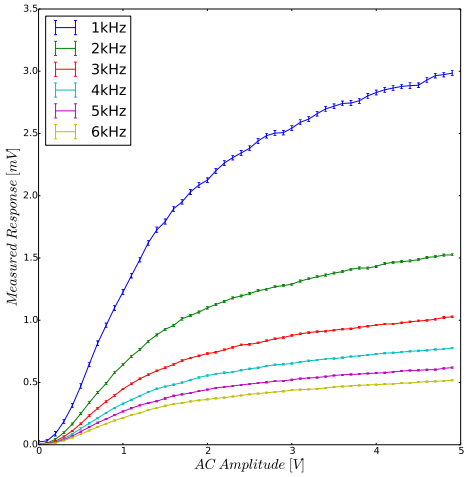

(b) $\omega_m + 2\omega_E$, JPK nano wizard III

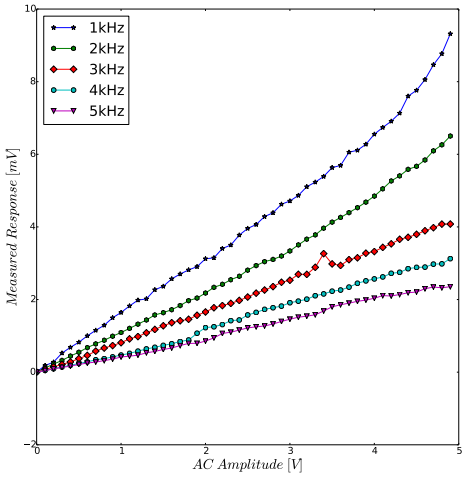

(c) $\omega_m + \omega_E$, low noise system

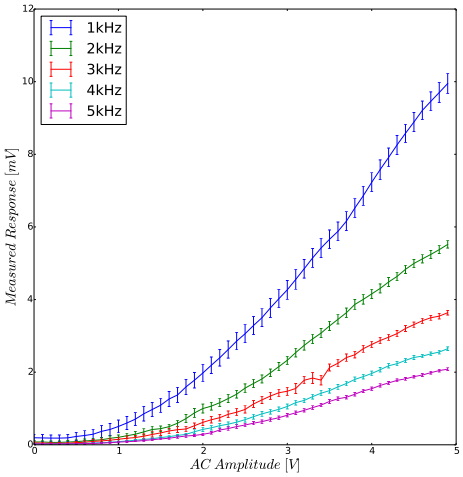

(d) $\omega_m + \omega_E$, low noise system

Fig. 4.4.: The measured response on the two harmonics on graphite in the open loop FM mode. Mention the negative slop on the JPK nano wizard III in the first harmonic as compared to the positive slope in the low noise system. This seems to be an effect of a phase jump, in the moment the cantilever leaves the attractive and enters the repulsive regime.

The dependence of the measured side band amplitudes on the AC excitation voltage provides additional ways to calculate the contact potential difference:
Since the first and second side band are linear and quadratic in the AC excitation voltage a fit of the following form could be performed:

$$\begin{aligned} A_{\omega_m+\omega_E} &= m_1 \cdot U_{Ac} \\ A_{\omega_m+2\omega_E} &= m_2 \cdot U_{Ac}^2 \end{aligned}$$

By using the equations from the theory chapter, equations 2.24 and 2.25, w.o.l.g. $\phi_E = 0$:

$$\begin{aligned} A_{\omega_m \pm \omega_E} &= \frac{1}{2 \cdot g(\omega_m+\omega_E)} a_1 U_{CPD} U_{AC} \\ A_{\omega_m \pm 2\omega_E} &= \frac{1}{8 \cdot g(\omega_m+2\omega_E)} a_1 U_{AC}^2 \end{aligned}$$

the following identification for m_1 and m_2 can be found, with the transfer function $g(\omega)$:

$$m_1 = g(\omega_m + \omega_E)^{-1} \cdot \frac{1}{2} a_1 U_{CPD} \tag{4.2}$$

$$m_2 = g(\omega_m + 2\omega_E)^{-1} \cdot \frac{1}{8} a_1 \tag{4.3}$$

Since the measurements were done for different electrical excitation frequencies ω_E, pairs of different frequencies can be found in this way, that $\omega_{E,1}$, electrical excitation frequency of the first side band, and $\omega_{E,2}$, electrical excitation frequency of the second side band, fulfil the following equation:

$$\omega_{E,1} = \omega_{E,2} \cdot 2$$

In this case the transfer function in equation 4.2 should have the same value as the transfer function in equation 4.3. So calculating $\frac{m1}{m2 \cdot 4}$ for this pairs should result in U_{CPD} without the need to take a certain value for the transfer function into account. The U_{CPD} calculated in this way can then be compared with the U_{CPD} calculated with the ratio of m_1 and m_2 on the same electrical excitation by taking the ratio of the transfer function of the driven harmonic oscillator into account. If there is a significant deviation between these two U_{CPD}, could this provide a evidance of a possible additional frequency dependency of the transfer function, as mention in 4.1.
This procedure was done for the measurement on the graphite sample in the low noise set up, the corresponding frequencies are $1\,kHz$ for m_2 combined with $2\,kHz$ for m_1 and $2\,kHz$ for m_2 combined with $4\,kHz$ for m_1. The fitted slopes are listed in the table 4.3, the U_{CPD} calculated with the alternative way are listed in 4.4. The two values are close to each other with a mean value of $650\,mV$, and the deviations could be caused by lateral drift of the cantilever. The U_{CPD} calculated with the ratio of the transfer function are listed in 4.5. As it can be seen in the plot of the U_{CPD} against the different electrical excitation frequencies 4.5, the value for U_{CPD} calculated with the ratio of the transfer function was not stable, but increased from a value of $564\,mV$ to a final value of $1.04\,V$. The slope of the function of the U_{CPD} against the electrical excitation frequency also seems to be decreasing, so that the value of U_{CPD} seems to be saturating against a final value, which is more than 50% higher than the mean value of the U_{CPD} calculated with the alternative way.

ω_E $[kHz]$	m_1 $[\cdot 10^-3]$	m_2 $[V^{-1} \cdot 10^-3]$
1	1.664 ± 0.014	0.445 ± 0.003
2	1.206 ± 0.011	0.249 ± 0.002
3	0.844 ± 0.003	0.164 ± 0.001
4	0.626 ± 0.005	0.118 ± 0.001
5	0.49 ± 0.003	0.092 ± 0.001

Table 4.3.: Fit slopes of the measurement on graphite without feedback. The r^2 values were all in the range of 0.99

frequency $[kHz]$	$U_{CPD,1}$ $[V]$
1& 2	0.678 ± 0.08
2& 4	0.629 ± 0.08

Table 4.4.: Calculated U_{CPD} by cancelling out the transfer function.

frequency $[kHz]$	$U_{CPD,2}$ $[V]$
1	0.564 ± 0.08
2	0.808 ± 0.08
3	0.920 ± 0.08
4	0.996 ± 0.08
5	1.036 ± 0.08

Table 4.5.: Calculated U_{CPD} by taking the transfer function into account.

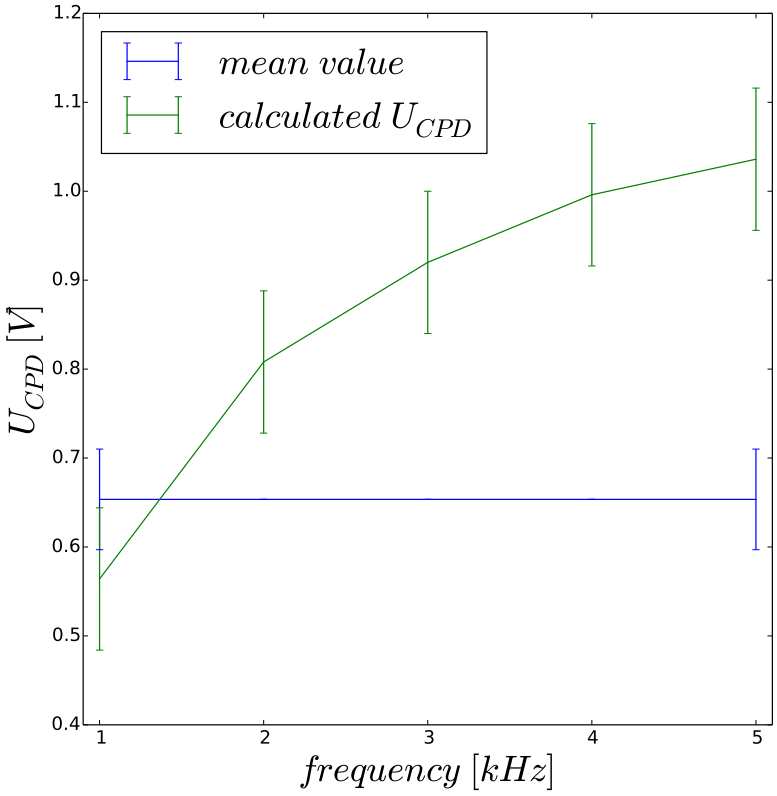

Fig. 4.5.: Graphical representation of the tabular 4.4 and 4.5. The blue line is the average of the two values calculated in 4.4. The green line are the points calculated in 4.5. The slope of the blue line also seems to be decreasing.

4.3. Height Dependency of U_{CPD}

The theory used to derive the equations for the methods do not predict any dependency of the tip sample distance for the measured U_{CPD}. That means, that the measured U_{CPD} should be constant by varying the tip-sample distance, and the following experiment was done to see if the different KPFM methods could fulfil this expectation. For this measurement the hover-mode was used, which first scans the topology on the trace direction and then follows this scanned topology on the retrace without an additional distance feedback on a user given distance. So for every distance step a picture was recorded, all pictures are listed in B.2, starting from a distance of $0\,nm$ to $150\,nm$. The averaging of the high and low electrodes was done by masking the electrodes of interest and calculating the mean and standard deviation for the masked area. Since the different KPFM methods were tested on different days, various cantilever were used, and the scanning area was dissimilar, the absolute values of the resulting measured potential difference of the different techniques could not be compared, however, the general trend of each of them can be discussed.

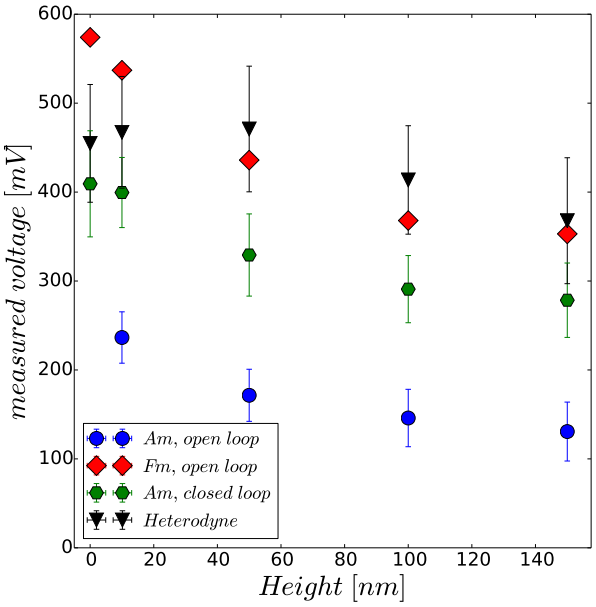

Fig. 4.6.: measured voltage from the four methods by different distance to the surface.

method	ω_m $[kHz]$	ω_E $[kHz]$	U_{AC} $[V]$
AM, closed loop	64.15	400.9	0.5
Heterodyne	63.2	332.0	2
AM, open loop	63.2	5	2
FM, open loop	63.13	1	6

Table 4.6.: Configuration for the height dependency measurements, ω_m, ω_E: mechanical and electrical excitation frequency, U_{AC}: AC excitation amplitude

The configuration of the set-up for these measurements are listed in 4.6, the voltage applied to the electrodes was $500\,mV$. In the plot 4.6 measured potential difference for the four KPFM methods are plotted against the hover-mode height. All measured U_{CPD} values decreased with higher tip-sample distance, except the heterodyne method, which first increases to a maximal value of $471\,mV$ at a distance of $50\,nm$ and then decreased to a value of $368\,mV$. The open loop FM methods measured a value of $574\,mV$ with a distance of $0\,nm$ and then decreased to a value of $353\,mV$. The closed and open loop AM method showed a similar trend as the FM open loop, with a starting value of $409\,mV$ and a end value of $278\,mV$, closed loop, and a starting value of $236\,mV$ and a end value of $146\,mV$, open loop. As in the measurement with the different applied voltages on the electrodes, 4.1, the open loop AM method reproduced much less of the applied potential difference. So this low efficiency is not a effect of a feedback crosstalk with the distance feedback, since the hover-mode works without this additional feedback loop. Another interesting thing is the fact, that the open loop FM method measured for small distances a value higher than the applied potential difference, then falls below the $500\,mV$ around a distance of $50\,nm$ and reproduced a similar value as the heterodyne method. Since we assumed a harmonic oscillation to derive the equations for the open loop method, section 2.3, this could be wrong for this small distances, where the cantilever starts to feel the strong repulsive forces.

4.4. Electronic Calibration

To exclude spurious signals or additional resonance frequencies in the transfer function of the system, especially some additional peaks in the lower range of the excitation frequencies, a sweep of the electrical excitation frequency was done from $100\,Hz$ to $100\,kHz$ with an AC excitation amplitude of $2\,V$ and a mechanical excitation of $63.06\,kHz$. During this sweep the amplitude of the first, ω_E, and the second harmonic, $2\omega_E$, was recorded, while the tip was positioned at the surface. On the plot of the first harmonic, fig. 4.7(a), there is no spurious signal in the lower regime of the frequencies, the only thing to mention here is the unusual decreasing after the mechanical excitation frequency, which could be an effect of crosstalk between the distance feedback and the electrical excitation. However, since the electrical excitation of the open loop methods was always small as compared to the mechanical excitation, $\omega_E \ll \omega_m$, the distribution in this area seems to be rather flat. The same discussion holds for the second harmonic $2\omega_E$, which is plotted in 4.7(b). In this plot the resonance peak appears at a lower frequency, and also in the regime where $\omega_E \ll \omega_m$ holds, the distribution was rather flat.

Since no spurious signal or additional resonance peak appears in the low frequency regime, there is still no explanation of the reproducible low measured potential difference between the electrodes by the open loop AM method.

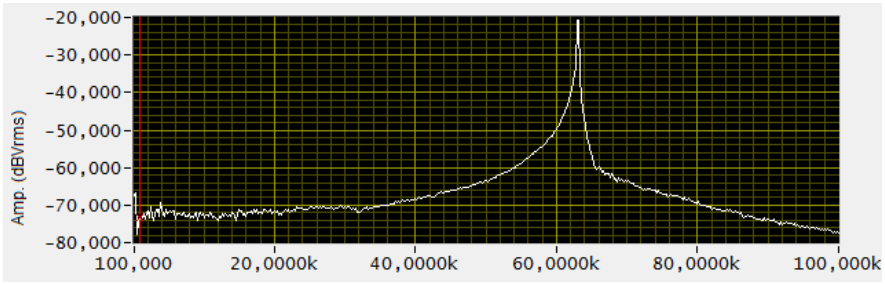

(a)

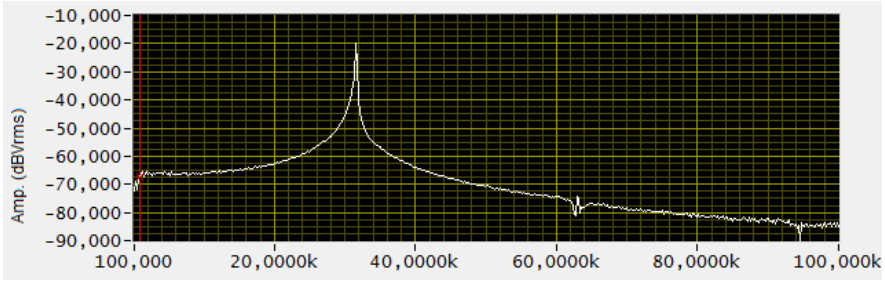

(b)

Fig. 4.7.: The measured response of the two side bands on the open loop am method, with ω_E: 4.7(a) and $2\omega_E$: 4.7(b) on different electrical excitation.

4.5. Possible Error Cause in Open Loop AM

After identifying different problems for open loop FM, the deviation of the value measured with the open loop AM is still not understood. However, there was some effects worth to discuss. Going back to the measurement that was done in 4.1, where over 25 lines different voltages were applied to the electrodes. In the topology scan, 4.9(a), was a change of the measured height on the electrode with the high potential at higher applied voltages, upper end of the picture. At the same time, a change in the amplitude of the second harmonic, $A_{2\omega_E}$, happened, 4.9(c). By using the equation for the amplitude of the second harmonic, equation 2.23, the amplitude should only depend on the gradient of the capacity and the AC excitation amplitude. The change of the amplitude measured over the electrode is plotted along the high electrode 4.8(a) and the low electrode 4.8(b) in 4.8. As it can be seen, the deviation is in the range of $10\,mV$ increasing for the low electrode and $70\,mV$ decreasing for the high electrode. This effect seems to be very small.

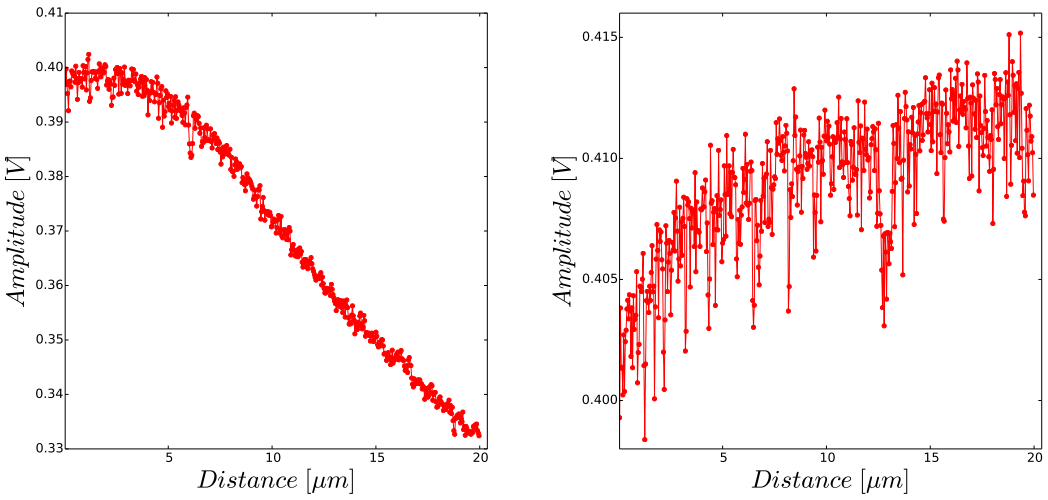

(a) high electrode

(b) low electrode

Fig. 4.8.: The cross sections are taken along the electrodes for amplitude of the second harmonic of the open loop AM measurement from 4.1. The applied voltage on the electrodes increased with higher distance.

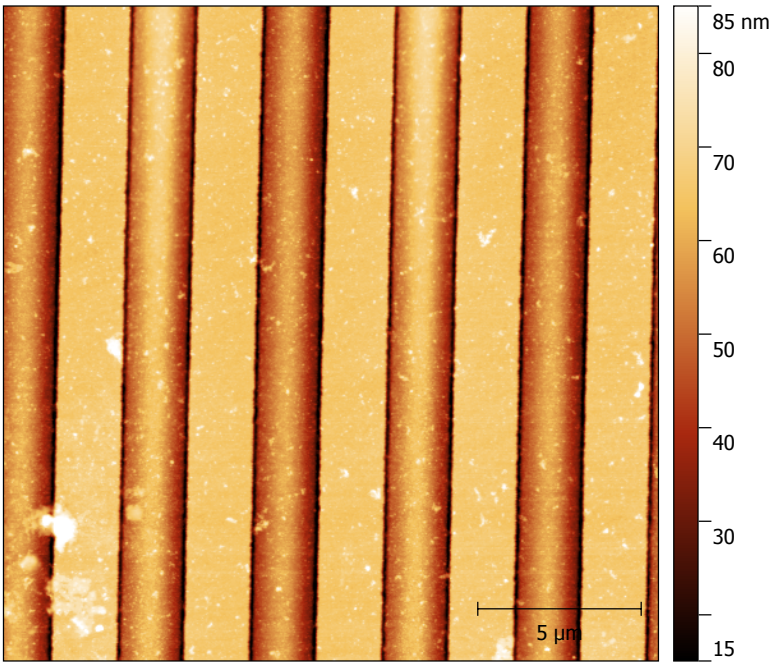

(a) Topology scan

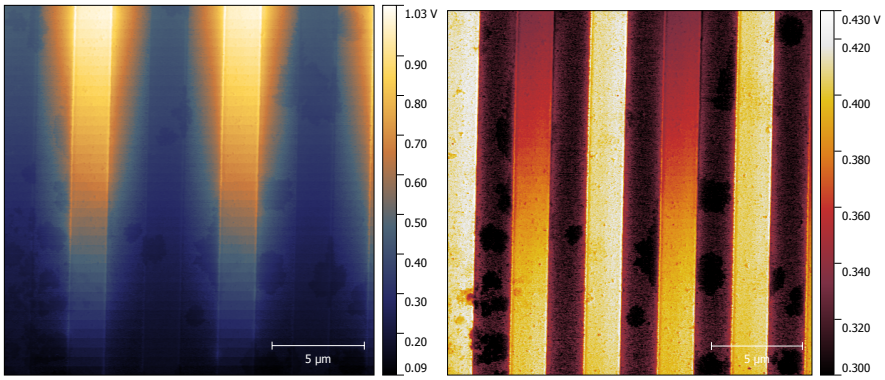

(b) First harmonic amplitude (c) Second harmonic amplitude

Fig. 4.9.: (a) topology scan for the measurement of the U_{CPD} with increasing electrode voltages in open loop AM mode. (b) amplitude of the first harmonic, (c) amplitude of the second harmonic

For an example the following calculation was done: By taking the cross section respectively for the amplitude of the first and second harmonic perpendicular to the electrodes for the highest electrode voltage, $3.8\,V$, the ΔU can be calculated, fig. B.6. The values for the amplitude on the second harmonic are for the low electrode: $0.41\,V$, for the low electrode: $0.33V$, for the amplitude of the first harmonic: for the high electrode: 0.42, for the low electrode: $0.98\,V$. From this follows, with the ration of the transfer function being 1 and with an AC excitation amplitude of $4\,V$:

$$\Delta U = (\frac{0.98}{0.33} - \frac{0.42}{0.41})V = 1.98\,V$$

If the value for the amplitude of the second harmonic is now being substituted with the value for the low electrode:

$$\Delta U = (\frac{0.98}{0.41} - \frac{0.42}{0.41})V = 1.37\,V$$

The calculated vale becomes even lower. Other possibilities are that the high AC excitation amplitude of $4\,V$ caused that the amplitudes of the first and second harmonic left the linear and quadratic regime, as it happened for the open loop FM method. However, by taking a look at a measurement, where different AC excitation amplitudes were tested in the lift mode, B.7, it can be seen, that the measured U_{CPD} decreased for higher AC excitation amplitudes. One of the last possible origins for the deviation of the measured U_{CPD} from the expected value is, that there was some AC-coupling between the electrical excitation and the piezo, which mechanical excited the cantilever, in the form of some extra excitation of the piezo due to the alternating voltage in combination with a resonance of the piezo in the area of the electrical excitation, causing a additional stimulation of the cantilever, but with opposite phase resulting in a reduction of the total amplitude. This theory could not be proven in the framework of this work.

5. Conclusion and Outlook

It was possible to implement the different KPFM methods into the JPK, and it was possible to reproduce the expected value for a potential difference between the two electrodes in the case of the closed loop methods. The open loop methods showed strong deviation from the expected value, 4.1. During a deeper analysis of the open loop methods other problems were identified, as the height dependence 4.3, or the feedback problem, 4.2. It was also possible to find a feasible additional frequency dependency of the transfer function using a new way to analyse the amplitude for different AC excitation amplitudes and electrical excitation frequencies, also discussed in 4.2. This technique can also easily applied to the open loop AM method by measuring the first and second harmonic amplitude for an electrical excitation.
Since all the problems cause systematic errors, adding a multiplicative factor to the measured U_{CPD}, the methods worked in principle, insofar as they behaved linear for increasing contact potential differences, further work should focus on how to optimise these slopes of the measured voltage against the applied voltage for the open loop methods. To do this, a first step could be, to reduce the complexity of the sample and just use a single metal electrode. The big advantage of a sample like that is, that it has a simple geometry. Studies of the first and second harmonic of the open loop AM method and the first and second side band of the open loop FM method could therefore easily compared with simulations.
Another thing worth to examine would be if there is any difference between the upper side band, $\omega_m + \omega_E$ and $\omega_m + 2\omega_E$, and the lower side band, $\omega_m - \omega_E$ and $\omega_m - 2\omega_E$. In this work only the upper side band was used, since there was no possibility to stream all four amplitudes to the JPK controller, so a possible further work could be to find a way to detect all four amplitudes at once.
However, not only the lower side band was neglected but also the phase between the electrical signal and excitation. This phase was set to zero at the beginning of every measurement, while the tip was positioned over a more or less unknown point on the sample, so there is the possibility of a change in the phase during the scan. So to reach higher accuracy recording the phase could also be a object of interest. As one motivation was the testing the usability of the open loop methods, since they provide a technique to measure samples in fluids, the long term goal is to doing this analysis with a sample as the one used in this thesis in a fluid. Some dependencies worth to examine could be the choose of the electrical excitation, since the mechanical resonance frequency in water is much lower compared to the one in air, the condition of $\omega_E \ll \omega_m$ is harder to fulfil. So a better control of the bandwidth of the distance feedback and of the lock-in amplifier is necessary, to isolate the mechanical frequency and the two side band frequencies.

A. Heterodyne Derivation

Useful equations

Bessel-functions

For the Bessel-function of the first kind and of the nth order the following equation holds:

$$J_n(x) = \frac{1}{2\pi} \int_{-\pi}^{\pi} \exp\left\{i(n \cdot \tau - x \cdot \sin(\tau))\right\} dx \tag{A.1}$$

For negative n the following relation can be found:

$$J_{-n}(x) = (-1)^n \cdot J_n(x) \tag{A.2}$$

Trigonometry Relations

For the addition of 2 angles in a cosine the next formula can be derived:

$$\cos(\alpha + \beta) = \cos\alpha \cdot \cos\beta - \sin\alpha \cdot \sin\beta \tag{A.3}$$

Fourier-Sum

A function $f(t)$ with the Period $T = \frac{2\pi}{\omega}$, e.g. $f(t+T) = f(t)$, can be Fourier expanded in the following way:

$$f(t) = \sum_{n=-\infty}^{\infty} C_n \cdot \exp(in\omega t) \tag{A.4}$$

with the coefficients:

$$C_n = \frac{1}{T} \int_{-\frac{T}{2}}^{\frac{T}{2}} f(t) \cdot \exp(-in\omega t) dt$$

with the transformation:

$$\begin{aligned} \tau &= \omega \cdot t \\ \Rightarrow \quad & \begin{cases} dt &= \frac{d\tau}{\omega} \\ \tau_0 &= -\pi \\ \tau_1 &= \pi \end{cases} \end{aligned}$$

You get:

$$C_n = \frac{1}{2\pi} \int_{-\pi}^{\pi} f\left(\frac{\tau}{\omega}\right) \cdot \exp(-in\tau) d\tau \tag{A.5}$$

Derivation of the sidebands in heterodyne

Starting with the equation:

$$s(t) = A \cdot \cos\{\omega_c t + h \cdot \sin(\omega_m t)\}$$

With the relation A.3 and by calling $\alpha = \omega_c t$ und $\beta = h \cdot \sin(\omega_m t)$ the formula above can be written as:

$$s(t) = A(\cos(\omega_c t) \cdot \cos(h \cdot \sin(\omega_m t)) - \sin(\omega_c t) \cdot \sin(h \cdot \sin(\omega_m t)))$$

The function can be easily continued to a complex function:

$$\begin{aligned} \tilde{s}(t) &= A \cdot f(t) \cdot \exp(i\omega_c t) \\ \text{with: } f(t) &= \exp(ih \cdot \sin(\omega_m t)) \end{aligned}$$

$f(t)$ is periodic with $T = 2\pi$ so it can be expend like it was present in equation A.4 The coefficients are given by A.5:

$$\begin{aligned} C_n &= \frac{1}{2\pi} \int_{-\pi}^{\pi} \exp(ih \cdot \sin(\tau)) \cdot \exp(-in\tau) d\tau \\ &= \frac{1}{2\pi} \int_{-\pi}^{\pi} \exp(-i(n\tau - h \cdot \sin(\tau))) d\tau \end{aligned}$$

with $\tau \to -\tau$ you get:

$$\begin{aligned} C_n &= \frac{1}{2\pi} \int_{\pi}^{\pi} \exp(i(n\tau - h \cdot \sin(\tau))) d\tau \\ &= J_n(h) \end{aligned}$$

whereat the relation A.1 was used. so we get for $\tilde{s}(t)$:

$$\tilde{s}(t) = A \cdot \sum_{n=-\infty}^{\infty} J_n(h) \cdot \exp(in\omega_m t) \cdot \exp(i\omega_c t)$$

If $h \ll 1$ the following relation holds:

$$J_n(h) \approx \frac{h^n}{n!}$$

So the expansion can be snapped after the first order:

$$\begin{aligned} \tilde{s} &\approx A(\{J_0(h) + J_1(h) \cdot \exp(i\omega_m t) + J_{-1} \cdot \exp(-i\omega_m t)\} \cdot \exp(i\omega_c t)) \\ &= A(J_0(h) \cdot \exp(i\omega_c t) \\ &+ J_1(h) \cdot \exp(i(\omega_m + \omega_c)t) \\ &+ J_{-1}(h) \cdot \exp(i(\omega_c - \omega_m)t)) \end{aligned}$$

All we need to do is to take the real part of $\tilde{s}(t)$ and we get with the relation A.2:

$$s(t) \approx J_0(h) \cos(\omega_c t) + J_1(h)(\cos(\omega_m + \omega_c)t) - \cos(\omega_c - \omega_m)t))$$

B. Pictures

B.1. Voltage Sweep

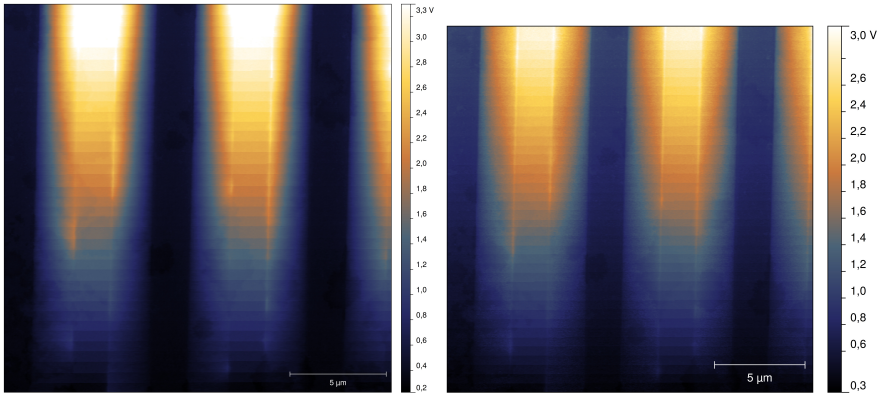

(a) closed loop AM

(b) open loop AM

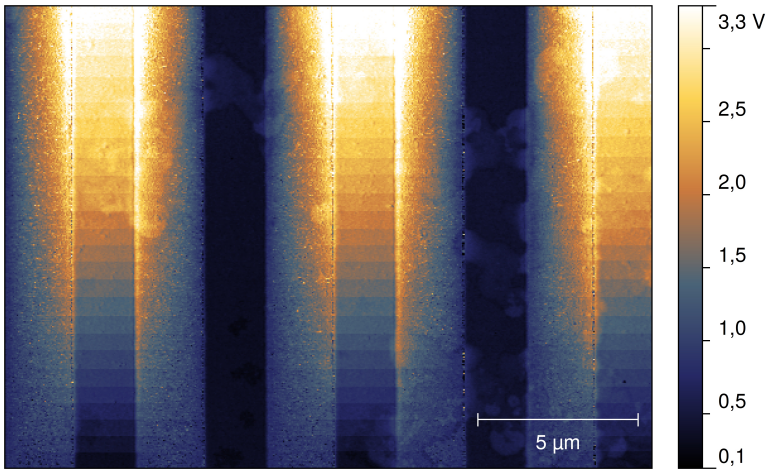

(c) open loop FM

Fig. B.1.: sweep of the applied voltage measured with the different techniques

B.2. Height Measurement

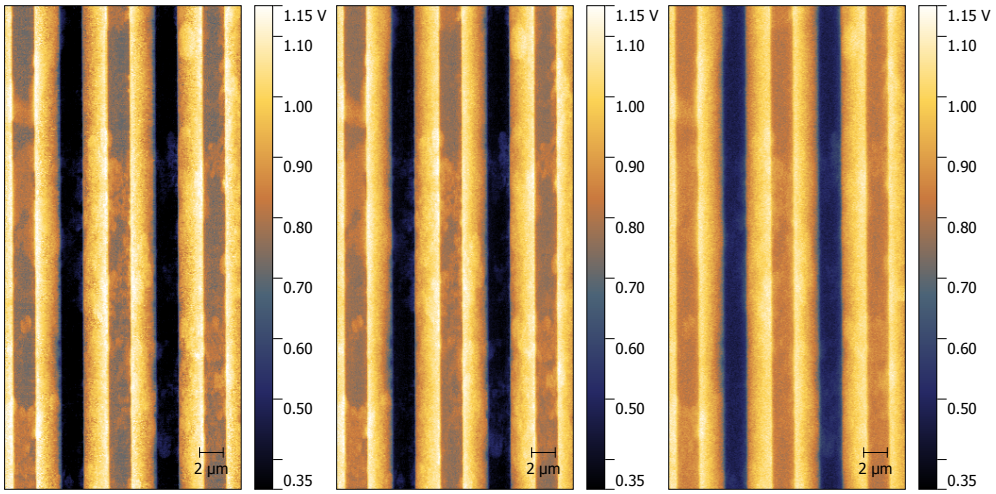

(a) $0nm$ (b) $10nm$ (c) $50nm$

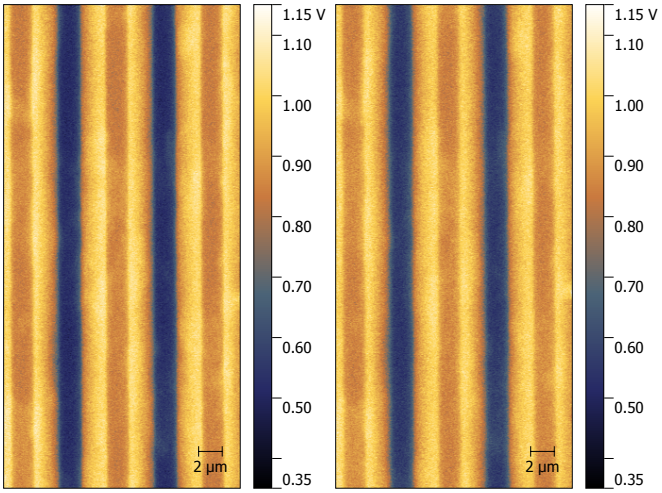

(d) $100nm$ (e) $150nm$

Fig. B.2.: Height measurements with the closed loop AM technique

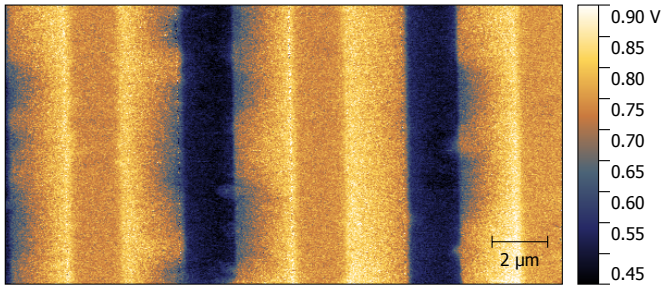

(a) $10nm$

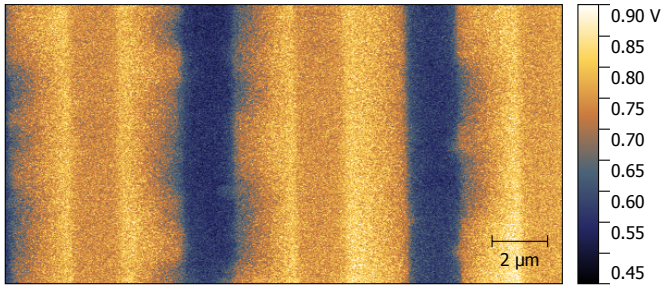

(b) $50nm$

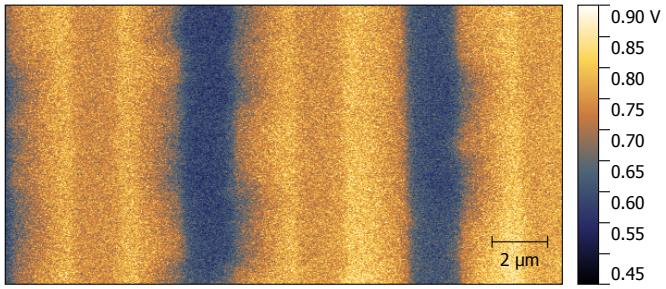

(c) $100nm$

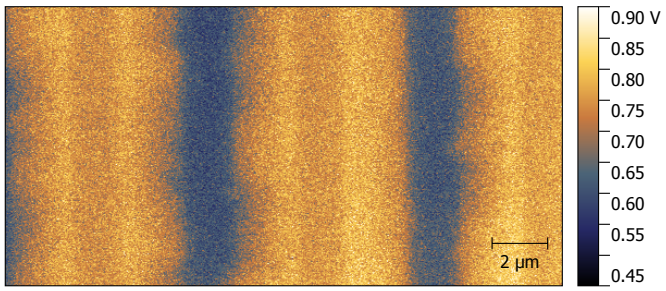

(d) $150nm$

Fig. B.3.: Height measurements with the open loop AM technique

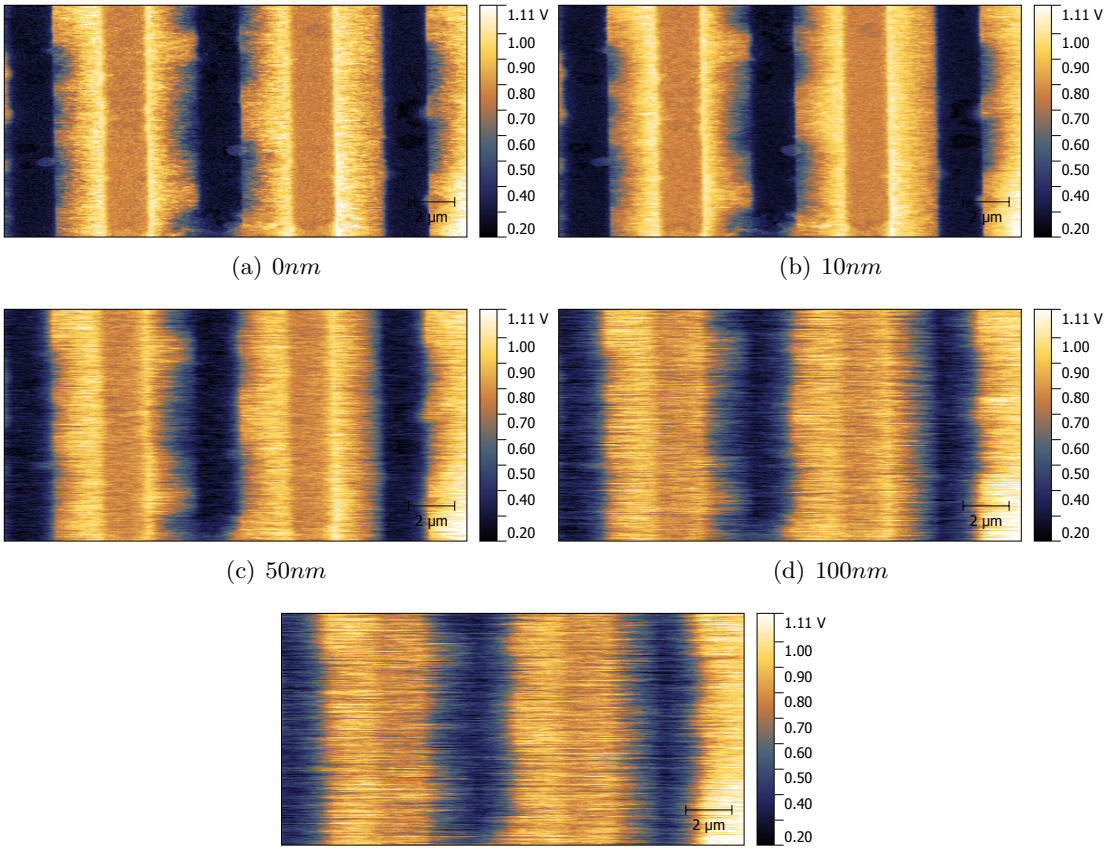

(a) $0nm$ (b) $10nm$

(c) $50nm$ (d) $100nm$

(e) $150nm$

Fig. B.4.: Height measurements with the closed loop FM technique

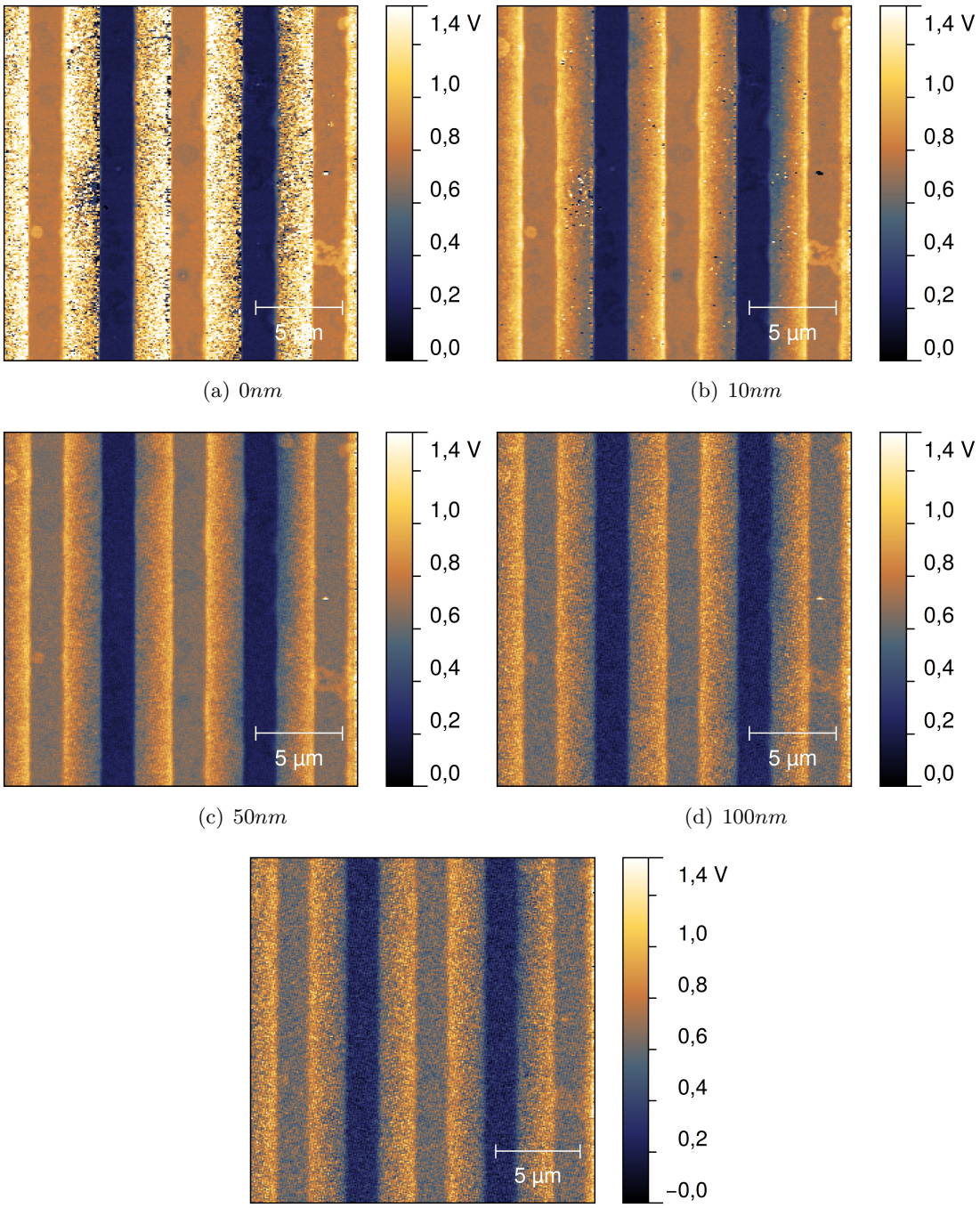

(a) 0nm (b) 10nm

(c) 50nm (d) 100nm

(e) 150nm

Fig. B.5.: Height measurements with the open loop FM technique

B.3. Open Loop AM Extra Pictures

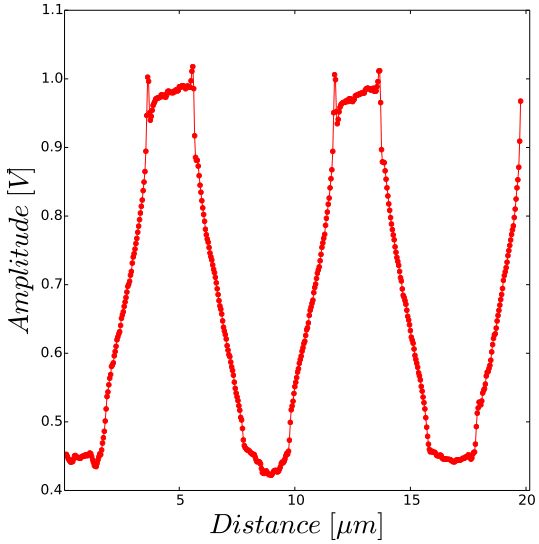

(a) Amplitude of the first harmonic

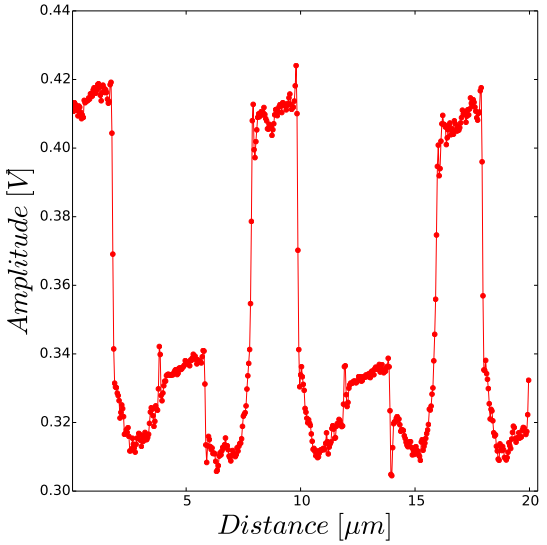

(b) Amplitude of the second harmonic

Fig. B.6.: Cross sections taken from the highest electrode voltage from the open loop AM measurement for increasing electrode voltages respectively for the amplitude on the first and the second harmonic, 4.1, averaged over 10 pixels, perpendicular to the electrodes.

method	ω_m $[kHz]$	ω_E $[kHz]$	h_{Hover} $[nm]$
AM, closed loop	64.2	400.9	10
Heterodyne	63.2	332.0	10
AM, open loop	63.2	5	10
FM, open loop	63.1	1	10

Table B.1.: Configuration for the AC excitation amplitude dependency measurements, ω_m, ω_E: mechanical and electrical excitation frequency, h_{Hover}: height of the hover mode

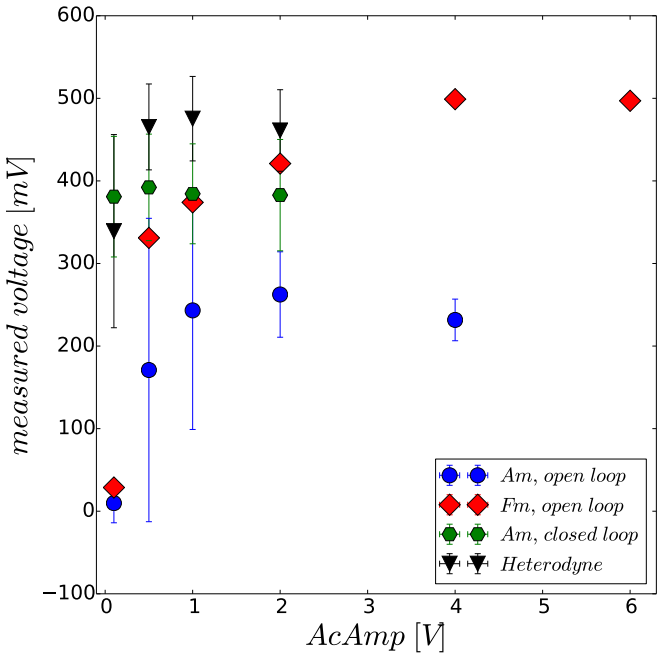

Fig. B.7.: Plot of the measured potential difference while $500mV$ voltage was applied to the electrodes against increasing AC excitation voltages, with hover mode on.

B.4. Pictures of the used Cantilevers

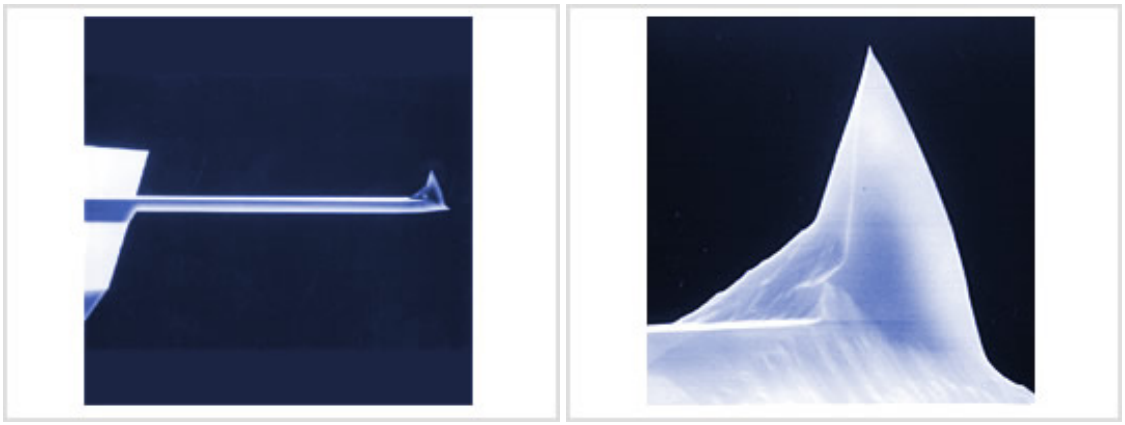

Fig. B.8.: The used Cantilevers, downloaded from brukerafmprobes.com on the 20.10.16.

C. Code

C.1. AC Amplitude Sweep

```
import zhinst.ziPython as ziPython  #Interface for the used LockIn amplifier
import zhinst.utils as utils    #Helperfuncion
import time
import numpy as np
import os

#Function to save a data array to a path into a text document of name
def save(data,path,name):
  if not os.path.exists(path):
    os.makedirs(path)
  output=open(path+name+'.txt','w')
  s=''
  for i in range(len(data)):
    s+=str(data[i])+'\n'
  output.write(s)
  output.close()

#used parameter
endFreq=5   #End frequency in kHz
endAmp=5    #End Ac amplitude in V
ampStep=0.1   #Ac amplitude increasing steps in V
pathName='folderToSave' #Save path

# Open connection to ziServer
daq = ziPython.ziDAQServer('localhost', 8005)

# Detect device
device = utils.autoDetect(daq)

#reading in the settings from a zicfg file, zicfg are config sheets produced by the software.
#Easy way to configurate the LockIn: -set the LockIn to state of operation by the software
#         -save zicfg
#The zicfg is not in a way the LockIn can handle, so some operation on the lines is necessary while reading in the lines.
#In every line is the first element the node and the second the value this node holds.
reader=open('yourConf.zicfg','r')
x=[]
y=[]
```

```
reader.readline()          #First line could be left out
for line in iter(lambda: reader.readline(),''):

  if len(line.split()) is not 0:
    x.append('/'+line.split()[0].lower()) #Need to convert capital letters
    to small letters for nodes
    temp=line.split()[1].replace(',','.') #Node value
    if temp.find('000000') is not -1: #Int value in the case a Int is
    needed
      y.append(int(temp[:-7]))
    else:
      y.append(float(temp))
  else:
    print('Kein Element vorhanden')
reader.close()

#getting the settings in the right form, so the lock in can handle them.
general_setting=[]
for i in range(len(x)):
  temp=[['/',device,x[i]],y[i]]
  general_setting.append(temp)

#set the settings
daq.set(general_setting)
time.sleep(1)
daq.flush()

#getting the data
path0='/'+device+'/demods/1/sample' #First harmonic in FM mode, change 1->0
     for AM
path1='/'+device+'/demods/2/sample' #Second harmonic in FM mode, change
    2->1 for AM

#Uncommend in the case the lower sidebands should be recorded too
#path2='/'+device+'/demods/4/sample'
#path3='/'+device+'/demods/5/sample'

daq.subscribe(path0)      #preparing the recording
daq.subscribe(path1)


#daq.subscribe(path2)
#daq.subscribe(path3)

#Initialization
amp=0.0   #Starting amplitude in V
freq=1    #Starting frequency in kHz


rangeAmp=daq.getDouble('/'+device+'/sigouts/0/range') #getting the output
    range in percent


```

```
86 for i in range(1,endFreq):  #for starting at another freq 1-> custom start
       freq
87   amp=0.0      #for every frequency the amplitude is setted to 0
88   freq=i+1     #frequency is increased by one kHz in every step
89   daq.setDouble('/'+device+'/oscs/0/freq',freq*10**3) #Setting the new
       values for excitation
90   daq.setDouble('/'+device+'/sigouts/0/amplitudes/6',amp) #and amplitude
91
92   for j in range(int(endAmp/ampStep)):
93     daq.flush()   #cleaning the memory
94     dataDict=daq.poll(5,500)#collecting data for 5 sec
95     #calculating the interested data sets and saving in numpy arrays.
96     #x2,r2 can be used for the lower sidebandes
97     x1=dataDict[device]['demods']['1']['sample']['x']
98     r1=np.sqrt(dataDict[device]['demods']['2']['sample']['x']**2+dataDict[
       device]['demods']['2']['sample']['y']**2)
99
100    #x2=dataDict[device]['demods']['4']['sample']['x']
101    #r2=np.sqrt(dataDict[device]['demods']['5']['sample']['x']**2+dataDict[
       device]['demods']['5']['sample']['y']**2)
102
103    #saving the data to a easily readable directory hierarchy
104    save(x1,pathName+'firstHarm/'+str(freq)+'kHz/',str(amp).replace('.','_'
       )+'V')
105    save(r1,pathName+'secHarm/'+str(freq)+'kHz/',str(amp).replace('.','_')+
       'V')
106
107    #save(x2,pathName+'lowerSideband/firstHarm/'+str(freq)+'kHz/',str(amp).
       replace('.','_')+'V')
108    #save(r2,pathName+'lowerSideband/secHarm/'+str(freq)+'kHz/',str(amp).
       replace('.','_')+'V')
109
110    amp+=ampStep    #increasing the amplitude by one step
111
112    daq.setDouble('/'+device+'/sigouts/0/amplitudes/7',amp/rangeAmp) #set
       the new amplitude for the next loop step
113
114    daq.flush()   #cleaning the memory for the next step.
115
116
117 daq.unsubscribe(path0)
118 daq.unsubscribe(path1)
119 #daq.unsubscribe(path2)
120 #daq.unsubscribe(path3)
```

D. Acknowledgement

„I know that I know nothing!“, with this famous words I want to close my thesis. And that is exactly the way I feel now after this weeks of work, but not in a negative way. As I started this work I was well enthusiast to finish the measurements quick and to focus on a good analysis, but I was disabused.
And at this point I want do start to thank my supervisor **Stefan Weber** for helping me to understand the magic of AFM and KPFM. On some days nothing seemed to worked, but he was always there to help, sometimes it just helps when he walks into the room (it was really a kind of magic..). So thank you for welcoming me in your group and guiding me through this work!
I also would like to thank Prof. **Angelika Kühnle** for accepting to be my second supervisor and for the great input from her and her group.
Furthermore i want thank all the people of group of Stefan Weber and the neighbour office for nice inputs and off topic talks, especially **Chris Goart** who was forced to share one desk with me.
I want to express my gratitude to all of my friends, which supported me during this time and always came forward to drink some beers and have some distracted evenings. Here I also want to thank my fellow students, which bear me from the very first day of university, when I was a naive young boy. There were a lot of funny conversations, which made the daily routine of learning and processing work sheets much more tolerable.
At last I want to thank my parents and my brother, which stand by my side, supporting me during my hole live.
So at the beginning I had known nothing, and now I still know nothing, but I learned a lot, and I am proud to had the opportunity to learn it in this nice environment.

Bibliography

[1] D. M. Chapin, C. S. Fuller, and G. L. Pearson.
A new silicon p–n junction photocell for converting solar radiation into electrical power.
Journal of Applied Physics, 25(5):676–677, 1954.

[2] Akihiro Kojima, Kenjiro Teshima, Yasuo Shirai, and Tsutomu Miyasaka.
Organometal halide perovskites as visible-light sensitizers for photovoltaic cells.
Journal of the American Chemical Society, 131(17):6050–5051, 2009.

[3] Henry J. Snaith, Antonio Abate, James M. Ball, Giles E. Eperon, Tomas Leijtens, Nakita K. Noel, Samuel D. Stranks, Jacob Tse-Wei Wang, Konrad Wojciechowski, and Wei Zhang.
Anomalous hysteresis in perovskite solar cells.
The Journal of Physical Chemistry Letters, 5(9):1511–1515, 2014.

[4] E. L. Unger, E. T. Hoke, C. D. Bailie, W. H. Nguyen, A. R. Bowring, T. Heumuller, M. G. Christoforo, and M. D. McGehee.
Hysteresis and transient behavior in current-voltage measurements of hybrid-perovskite absorber solar cells.
Energy Environ. Sci., 7:3690–3698, 2014.

[5] Lord Kelvin.
V. contact electricity of metals.
Philosophical Magazine Series 5, 46(278):82–120, 1898.

[6] G. Binnig, C. F. Quate, and Ch. Gerber.
Atomic force microscope.
Phys. Rev. Lett., 56:930–933, 1986.

[7] M. Nonnenmacher, M. P. O'Boyle, and H. K. Wickramasinghe.
Kelvin probe force microscopy.
Applied Physics Letters, 58(25):2921–2923, 1991.

[8] L. Garrett Joseph and N. Munday Jeremy.
Fast, high-resolution surface potential measurements in air with heterodyne kelvin probe force microscopy.
Nanotechnology, 27(24):245705, 2016.

[9] Riccardo Borgani, Daniel Forchheimer, Jonas Bergqvist, Per-Anders Thorén, Olle Inganäs, and David B. Haviland.

Intermodulation electrostatic force microscopy for imaging surface photo-voltage.
Applied Physics Letters, 105(14):143113, 2014.

[10] L Collins, J I Kilpatrick, S A L Weber, A Tselev, I V Vlassiouk, I N Ivanov, S Jesse, S V Kalinin, and B J Rodriguez.
Open loop kelvin probe force microscopy with single and multi-frequency excitation.
Nanotechnology, 24(47):475702, 2013.

[11] Kei Kobayashi and Hirofumi Yamada.
Frequency Modulation Atomic Force Microscopy in Liquids, chapter 15, pages 303–328.
Springer, 2009.

[12] Gerd Czycholl.
Nicht wechselwirkende Elektronen im Festkörper, chapter 4, pages 127–128.
Springer, 2008.

[13] Rudolf Gross and Achim Marx.
Das freie Elektronengas, chapter 7, pages 279–282.
Oldenbourg Verlag München, 2012.

[14] Stefan Weber.
Electrical Scanning Probe Microscopy on Organic Optoelectronic Devices.
dissertation, Johannes-Gutenberg-University Mainz, 2010.

[15] Ulrich Zerweck, Christian Loppacher, Tobias Otto, Stefan Grafström, and Lukas M. Eng.
Accuracy and resolution limits of kelvin probe force microscopy.
Physical Review B, 71(12):125424, 2005.

[16] Hagen Söngen, Philipp Rahe, Julia L. Neff, Ralf Bechstein, Juha Ritala, Adam S. Foster, and Angelika Kühnle.
The weight function for charges—a rigorous theoretical concept for kelvin probe force microscopy.
Journal of Applied Physics, 119(2), 2016.

List of Figures

List of Tables